

DOCUMENT CONTROL DATA - R & D

(Security classification of title, body of abstract and indexing annotation must be entered when the overall report is classified)

744776

1. ORIGINATING ACTIVITY (Corporate author) Harry Diamond Laboratories Washington, D. C. 20438	2a. REPORT SECURITY CLASSIFICATION UNCLASSIFIED
	2b. GROUP

3. REPORT TITLE
RESPONSE OF AN AIRBORNE-SHORT-PULSE RADAR TO CHAFF

4. DESCRIPTIVE NOTES (Type of report and inclusive dates)

5. AUTHOR(S) (First name, middle initial, last name)
James E. Seltzer

6. REPORT DATE April 1972	7a. TOTAL NO. OF PAGES 58	7b. NO. OF REFS 11
------------------------------	------------------------------	-----------------------

8a. CONTRACT OR GRANT NO. b. PROJECT NO. HDL JCM14 c. AMCMS Code: 522A.11.17700 d. DA-1B262301A208	9a. ORIGINATOR'S REPORT NUMBER(S) HDL-TR-1590
	9b. OTHER REPORT NO(S) (Any other numbers that may be assigned this report)

10. DISTRIBUTION STATEMENT
Approved for public release; distribution unlimited

11. SUPPLEMENTARY NOTES	12. SPONSORING MILITARY ACTIVITY Army Materiel Command
-------------------------	---

13. ABSTRACT

Radar backscatter from a chaff cloud is examined for the case in which the radar approaches the cloud from above and moves into and through the cloud. The chaff cloud is modelled as a collection of randomly distributed and randomly oriented dipoles having a mean volume density that is a function of altitude but invariant in a horizontal plane. The statistics of the chaff echo power when the number of dipoles in the resolution volume is large are reviewed. The impulse response, which approximates the short-pulse radar response, and the radar return signal for a specific range resolution cell as a function of the position of the radar relative to the cloud are derived for several chaff cloud configurations and antenna patterns. Power spectral density functions for range-gated chaff-return signals and correlation functions for the signals following square-law detection are also derived.

14. KEY WORDS	LINK A		LINK B		LINK C	
	ROLE	WT	ROLE	WT	ROLE	WT
Chaff model	8	3				
Impulse response	8	3				
Chaff backscatter	8	3				
Dipole scatterer	8	3				

B

AD

DA-1B262301A208
AMCMS Code: 522A.11.17700
HDL Proj 1CM14

HDL-TR-1590
**RESPONSE OF AN AIRBORNE-SHORT-PULSE
RADAR TO CHAFF**

by
James E. Seltzer

April 1972



U.S. ARMY MATERIEL COMMAND
HARRY DIAMOND LABORATORIES
WASHINGTON, D.C. 20438

APPROVED FOR PUBLIC RELEASE; DISTRIBUTION UNLIMITED.

ABSTRACT

Radar backscatter from a chaff cloud is examined for the case in which the radar approaches the cloud from above and moves into and through the cloud. The chaff cloud is modelled as a collection of randomly distributed and randomly oriented dipoles having a mean volume density that is a function of altitude but invariant in a horizontal plane. The statistics of the chaff echo power when the number of dipoles in the resolution volume is large are reviewed. The impulse response, which approximates the short-pulse radar response, and the radar return signal for a specific range resolution cell as a function of the position of the radar relative to the cloud are derived for several chaff cloud configurations and antenna patterns. Power spectral density functions for range-gated chaff-return signals and correlation functions for the signals following square-law detection are also derived.

Preceding page blank

ACKNOWLEDGMENT

The author wishes to acknowledge the assistance of Dr. Valdis Liepa of the University of Michigan Radiation Laboratory, in developing the exponential density chaff cloud model as well as the fundamentals of the technique used in deriving the chaff impulse response function.

Dr. Liepa, during his stay at the Harry Diamond Laboratories, summarized the results of his investigation in an internal report; his results laid the foundation for the current study.

CONTENTS

	<u>Page</u>
ABSTRACT	3
ACKNOWLEDGMENT	4
1. INTRODUCTION	9
2. ENCOUNTER REFERENCE FRAME	9
3. CHAFF CLOUD MODEL	9
4. MEAN IMPULSE RESPONSE	21
4.1 Signal Return from a Single Scatterer	21
4.2 Signal Return from Volume-Distributed Scatterers	21
4.2.1 Scattering from a Semi-Infinite Cloud	23
4.2.2 Finite Thickness Chaff Layers	25
4.2.3 Varying Density Chaff	25
5. PROBABILITY DENSITY FUNCTIONS FOR CHAFF BACKSCATTER	31
6. POWER SPECTRAL DENSITY	35
7. CORRELATION FUNCTION	39
8. SUMMARY	42
9. LITERATURE CITED	42
GLOSSARY OF SYMBOLS AND ABBREVIATIONS	43
APPENDIX A.—Impulse Response Functions	47

ILLUSTRATIONS

<u>Figure</u>	<u>Page</u>
1 Encounter reference frame	10
2 Back scattering cross section of a wire parallel to electric vector; $a/\lambda = 6.27 \times 10^{-3}$	11
3 Measured backscattering cross section of a wire as a function of azimuth, ϕ ; $l/\lambda = 6.27 \times 10^{-2}$	12
4 Measured backscattering cross section of a wire as a function of azimuth angle, ϕ ; $l/\lambda = 6.27 \times 10^{-3}$	12
5 Geometry for computation of the cross section of a dipole	13
	5

ILLUSTRATIONS--(continued)

<u>Figure</u>		<u>Page</u>
6	Geometry for horizontal polarization calculations	14
7	Geometry for vertical polarization calculations	15
8	Mean backscatter cross section as a function of elevation angle (θ) of incident wave--horizontal polarization	16
9	Cross section of a semi-infinite chaff cloud	24
10	Impulse response functions at $h = 100$ m for an isotropic antenna pattern and uniformly distributed dipole orientations (exponential cloud model)	29
11	Impulse response functions at $h = 100$ m for a $\cos^2 \theta$ antenna pattern and uniformly distributed dipole orientations (exponential cloud model)	29
12	Impulse response functions at $h = 100$ m for a $\sin \theta \cos \theta$ antenna pattern and uniformly distributed dipole orientations (exponential cloud model)	29
13	Impulse response functions at $h = 100$ m for an isotropic antenna pattern, vertically polarized wave, and horizontally distributed dipole orientations (exponential cloud model)	29
14	Impulse response functions at $h = 100$ m for an isotropic antenna pattern and uniformly distributed dipole orientations (Rayleigh cloud model)	30
15	Impulse response functions at $h = 100$ m for a $\cos^2 \theta$ antenna pattern and uniformly distributed dipole orientations (Rayleigh cloud model)	30
16	Impulse response functions at $h = 100$ m for a $\sin \theta \cos \theta$ antenna pattern and uniformly distributed dipole orientations (Rayleigh cloud model)	30
17	Impulse response functions at $h = 100$ m for an isotropic antenna pattern, vertically polarized wave, and horizontally distributed dipole orientations (Rayleigh cloud model)	30
18	Range-gated response at $d = 100$ m for an isotropic antenna pattern and uniformly distributed dipole orientations (exponential cloud model)	32
19	Range-gated response at $d = 100$ m for a $\cos^2 \theta$ antenna pattern and uniformly distributed dipole orientations (exponential cloud model)	32
20	Range-gated response at $d = 100$ m for a single-lobe $\cos^2 \theta$ antenna pattern and uniformly distributed dipole orientations (exponential cloud model)	32
21	Range-gated response at $d = 100$ m for a $\sin \theta \cos \theta$ antenna pattern and uniformly distributed dipole orientations (exponential cloud model)	32
22	Range-gated response at $d = 100$ m for an isotropic antenna pattern, vertically polarized wave, and horizontally distributed dipole orientations (exponential cloud model)	33
23	Range-gated response at $d = 100$ m for an isotropic antenna pattern and uniformly distributed dipole orientations (Rayleigh cloud model)	33
24	Range-gated response at $d = 100$ m for a $\cos^2 \theta$ antenna pattern and uniformly distributed dipole orientations (Rayleigh cloud model)	33
25	Range-gated response at $d = 100$ m for a single-lobe $\cos^2 \theta$ antenna pattern and uniformly distributed dipole orientations (Rayleigh cloud model)	33

ILLUSTRATIONS--(continued)

<u>Figure</u>		<u>Page</u>
26	Range-gated response at $d = 100$ m for a $\sin \theta \cos \theta$ antenna pattern and uniformly distributed dipole orientations (Rayleigh cloud model)	34
27	Range-gated response at $d = 100$ m for an isotropic antenna pattern, vertically polarized wave, and horizontally distributed dipole orientations (Rayleigh cloud model)	34
28	Doppler spectral density function for range-gated response at $d = 100$ m with an isotropic antenna pattern (Rayleigh cloud model, $\alpha = 0.001$) uniformly distributed dipole orientations	38
29	Doppler spectral density function for range-gated response at $d = 100$ m with a $\cos^2 \theta$ antenna pattern (Rayleigh cloud model, $\alpha = 0.001$) uniformly distributed dipole orientations	39
30	Correlation function for range-gated response at $d = 100$ m with an isotropic antenna pattern (Rayleigh cloud model, $\alpha = 0.001$) uniformly distributed dipole orientations	41
31	Correlation function for range-gated response at $d = 100$ m with a $\cos^2 \theta$ antenna pattern (Rayleigh cloud model, $\alpha = 0.001$) uniformly distributed dipole orientations	41

1. INTRODUCTION

Radar systems are frequently required to operate in the presence of echoes from chaff, ground and sea surfaces, clouds, and the various forms of precipitation. To operate effectively in such environments, the radar must be designed to minimize the effects of these clutter signals which may lead to spurious detections, that is, false alarms, or to desensitization of the radar so that the actual target is shielded. A prerequisite for radar design optimization is a model for the clutter environment that is sufficiently general to cover the range of conditions likely to be encountered while retaining the simplicity essential to its utility as a design instrument.

This report examines a model for a chaff cloud consisting of a collection of randomly oriented and randomly distributed dipoles. Specifically considered is the response of an airborne radar transmitting a short pulse and moving rapidly relative to the chaff cloud. The impulse response function for chaff backscatter is derived, and the return from a fixed range is examined for a radar moving through the chaff. The results obtained are valid for narrow transmitted pulse widths and may be extended to cases involving wide pulses by convolving the transmitted pulse envelope with the impulse response function.

The first- and second-order probability density functions for chaff echo powers are reviewed, and the correlation and spectral density functions associated with this chaff model are derived.

2. ENCOUNTER REFERENCE FRAME

For the following discussion, it is assumed that the chaff cloud is confined to a specified region of space. In all cases the chaff cloud will be assumed bounded above by a plane surface parallel to the tangent plane to the mean surface of the earth. A Cartesian reference frame is constructed with the radar at the origin as shown in figure 1.

It is further assumed that the radar velocity is constant throughout the encounter which implies that the flight angle γ between the z-axis and the radar velocity vector is also constant.

The radar receives returns from chaff elements located in that portion of the spherical shell lying within the cloud and with boundaries at radial distances d and $d + \Delta d$ from the radar. The distance, h , from the radar to the upper edge of the cloud is positive when the radar is above the cloud top and negative when below. For a radar speed V , this distance varies during the encounter as

$$h = d - Vt \cos \gamma. \quad (1)$$

with the time origin taken as the time when the radar range gate first penetrates the cloud to a depth equal to the range gate width, Δd .

3. CHAFF CLOUD MODEL

The chaff cloud is assumed to consist of a collection of resonant dipoles, randomly oriented and randomly distributed within a volume, large relative to the radar resolution cell. It is further assumed that the dipole locations are statistically independent, so that the number

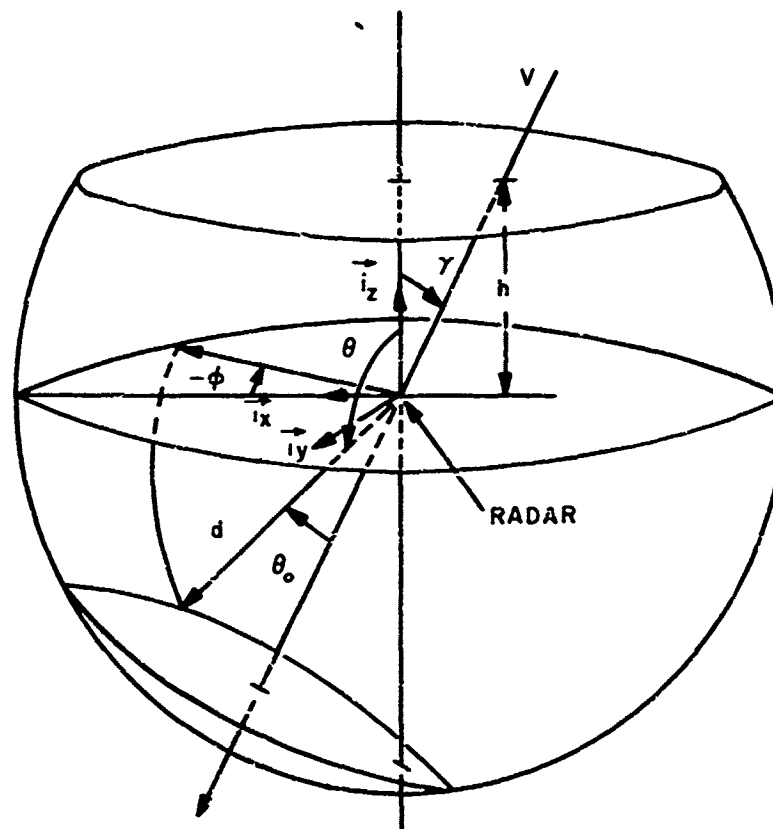


Figure 1. Encounter reference frame. (The distance h from the radar to the top of the chaff cloud is taken as positive when the radar is above the cloud top and negative when below).

of dipoles found in any subvolume is a Poisson distributed random variable. It should be noted that such a distribution does not account for the effect of chaff clumping, or "birdnesting."

Since we assume that the basic scatterer of the chaff cloud is a dipole, it is appropriate to look first at the scattering behavior of a single dipole. The radar backscatter from a dipole is usually maximum when the dipole is viewed at broadside with the electric vector of the incident wave parallel to the axis of the dipole. The magnitude of this return as a function of the length l of the dipole is shown in figure 2. At $l/\lambda \approx 0.45$, the curve shows a definite peak; Because of this resonant cross section enhancement, half-wave dipoles give the maximum return per unit length of the wire. Dipole thickness has a relatively small effect on the return; the general tendency being that the amount of resonant peaking is diminished for thicker dipoles.

As a dipole is rotated in the plane formed by the direction of incidence and the electric vector of the incident wave, the amplitude of the backscattered field changes. In figures 3 and 4, the radar cross sections are shown as functions of rotation for a half-wave resonant dipole ($l/\lambda \approx 0.452$) and for a dipole whose length is 2.46λ , respectively.¹ It may be observed that in the first case the cross section exhibits a single lobe; but for the longer dipole,

¹Chung, S. and Liepa, V., "Measured Back Scattering Cross Section of Thin Wires," The University of Michigan Radiation Laboratory, Report No. 8077-4-T, 1967.

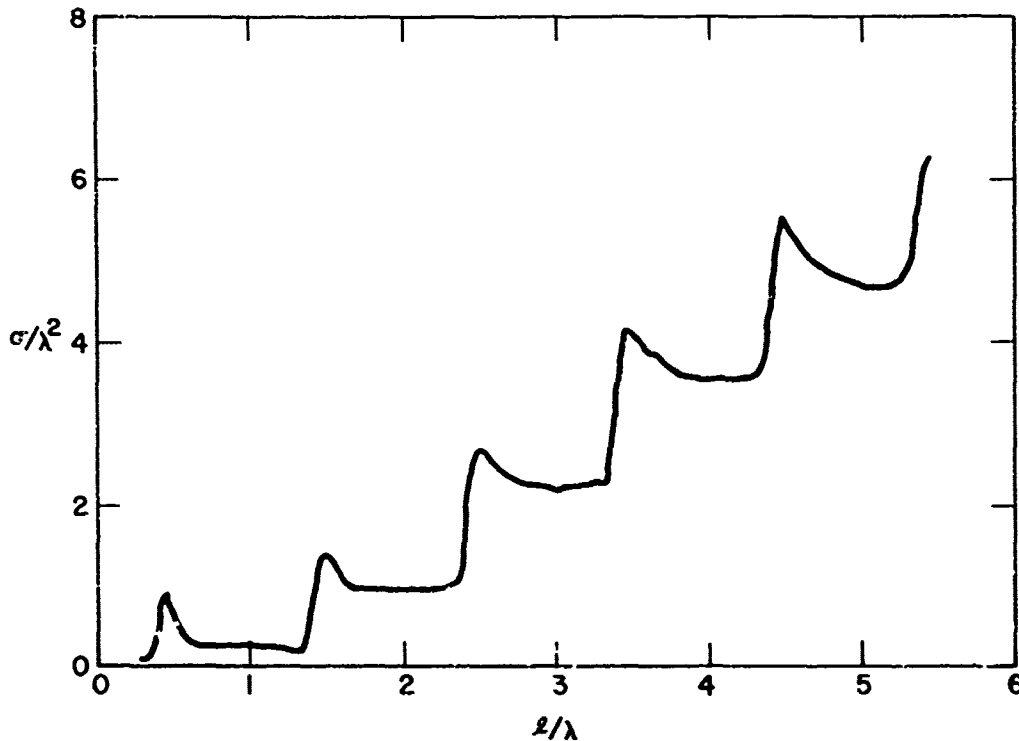


Figure 2. Backscattering cross section of a wire parallel to electric vector; $a/\lambda = 6.27 \times 10^{-3}$. (a = radius of wire, l = length of wire, λ = wavelength.)

multiple lobes appear. For certain lengths, the amplitude of the sidelobes may be greater than that of the broadside lobe. It may also be noted that in the case of the half-wave dipole the $|\sin^5 \phi'|$ curve provides a close empirical approximation to the experimental curve (fig. 3).

If the dipole is rotated in a plane perpendicular to the direction of incidence, a similar variation in radar cross section occurs. In this case the cross section has been found to vary as $\sin^4 \theta'$, where the angle θ' is defined in figure 5. Hence, we have the half-wave dipole radar cross section as a function of the polarization of the incident field (horizontal as depicted in picture fig. 5) and the dipole orientation along the two principal planes of rotation.

Accordingly, we can write

$$\left. \frac{\sigma(\theta', \phi')}{\lambda^2} \right|_{\theta' = \pi/2} = 0.89 |\sin^5 \phi'|. \quad (2)$$

$$\left. \frac{\sigma(\theta', \phi')}{\lambda^2} \right|_{\phi' = \pm \pi/2} = 0.89 \sin^4 \theta'. \quad (3)$$

²deBettancourt, J. T., "Bistatic Cross Sections of Cylindrical Wires," Pickard & Burns, Inc., Scientific Report No. 1, P&B Pub. No. 735A, Waltham, Mass., 1961.

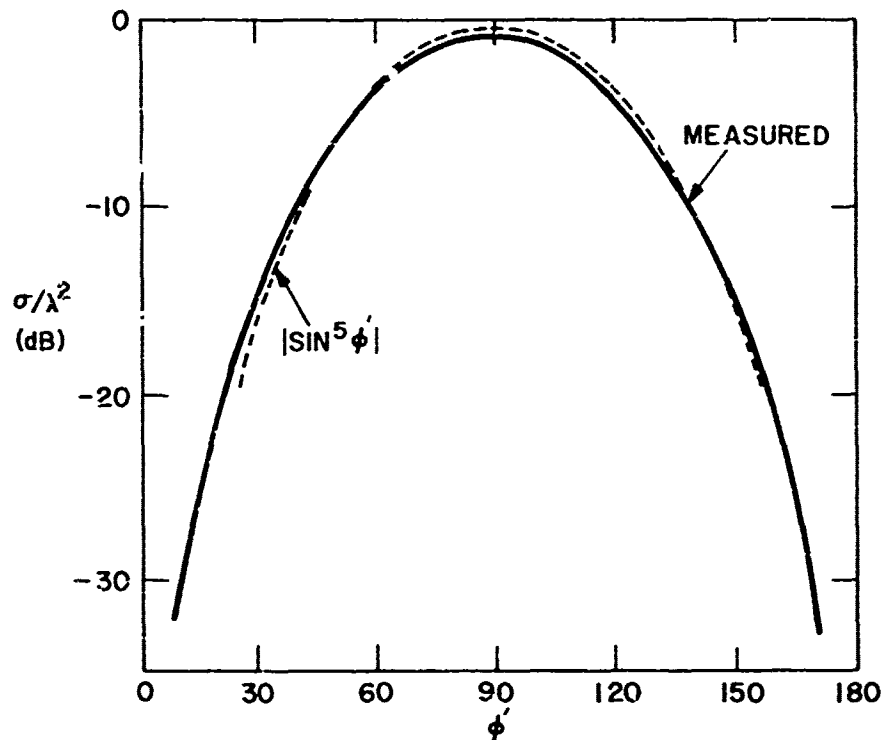


Figure 3. Measured backscattering cross section of a wire as a function of azimuth, ϕ' , $l/\lambda = 0.452$, $a/\lambda = 6.27 \times 10^{-2}$ (Chang and Liepa, 1967). The dotted curve shows how well $|\sin^5 \phi'|$ curve fits the measured data. [$\theta = 90^\circ$]. (a = radius of wire, l = length of wire, λ = wavelength.)

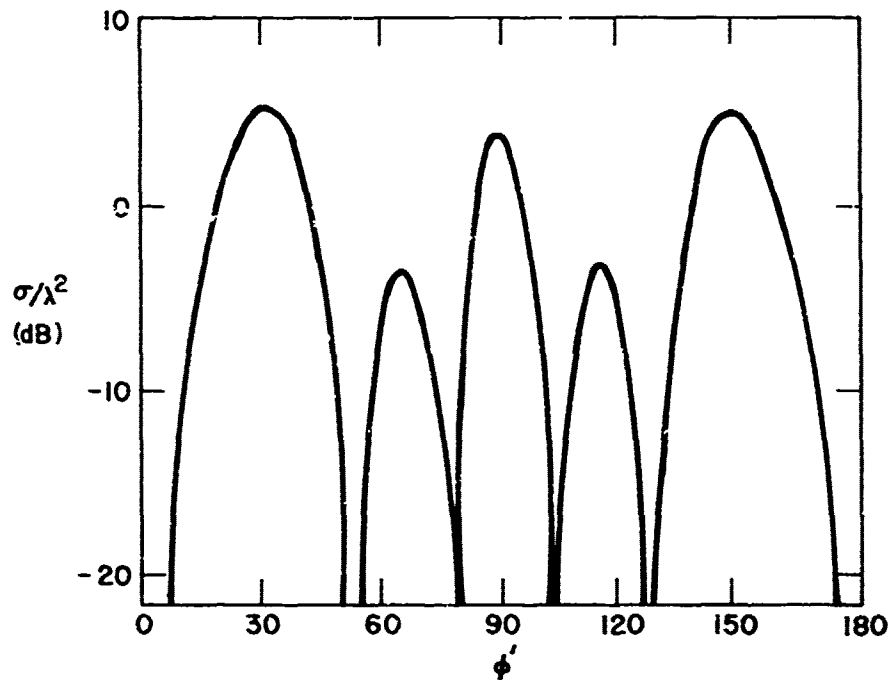


Figure 4. Measured backscattering cross section of a wire as a function of azimuth angle, ϕ' , $l/\lambda = 2.460$, $a/\lambda = 6.27 \times 10^{-3}$ (Chang and Liepa, 1967) [$\theta = 90^\circ$]. (a = radius of wire, l = length of wire, λ = wavelength.)

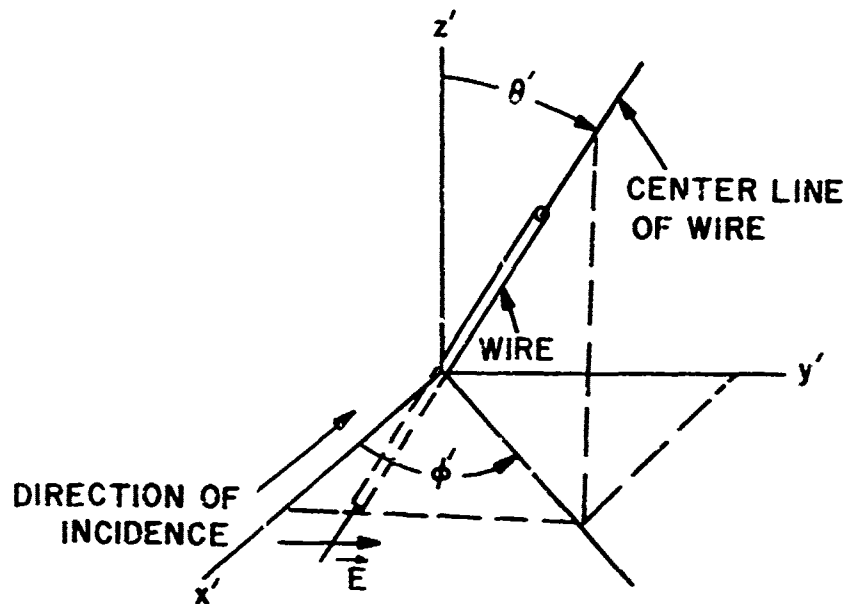


Figure 5. Geometry for computation of the cross section of a dipole.

Assuming that $\sigma(\theta', \phi') = 0.89 \lambda^2 \sigma_1(\theta') \sigma_2(\phi')$ where $\sigma_1(\theta') = \sin^4 \theta'$ and $\sigma_2(\phi') = |\sin^5 \phi'|$ which seems to be a valid approximation in the case of the half-wave dipole, we may combine equations (2) and (3) to obtain an empirical angular expression for a half-wave resonant dipole as

$$\frac{\sigma(\theta', \phi')}{\lambda^2} = 0.89 \sin^4 \theta' |\sin^5 \phi'|. \quad (4)$$

Since half-wave dipoles are most efficient in that they provide the maximum return per unit weight, we shall be concerned hereafter with such dipole lengths only.

In a chaff cloud consisting of a large number of dipoles, it is impossible to specify the orientation of each of the individual dipoles. We are therefore confronted with the problem of determining an average dipole cross section based on the probability density of dipole orientations. We consider two possible distributions: (a) uniformly distributed over 4π steradians, and (b) confined to a horizontal plane but uniformly distributed over 2π radians.

In case (a), the probability density of dipole orientations becomes

$$p(\theta', \phi') = \frac{1}{4\pi} \sin \theta' \begin{cases} 0 \leq \phi' < 2\pi \\ 0 \leq \theta' < \pi \end{cases} \quad (5)$$

The mean cross section per dipole is independent of incident polarization and direction of incidence and is obtained simply

$$\frac{\bar{\sigma}}{\lambda^2} = \frac{0.89}{4\pi} \int_0^\pi \int_0^{2\pi} |\sin^5 \phi'| \sin^4 \theta' \sin \theta' d\phi' d\theta' \quad (6)$$

$$= 0.162.$$

In case (b), the probability density of dipole orientation becomes

$$p(\Psi) = \frac{1}{2\pi} \quad 0 \leq \Psi < 2\pi, \quad (7)$$

where $\Psi = \Psi(\theta', \phi', \theta, \phi)$ is a random function of the direction of incidence (θ, ϕ) and the dipole orientation angles (θ', ϕ') with respect to a spherical reference frame centered on the dipole (figs. 6 and 7). The rotation angle Ψ is measured in a horizontal plane.

Considering first a horizontally polarized incident field, we obtain from figure 6 the following relations

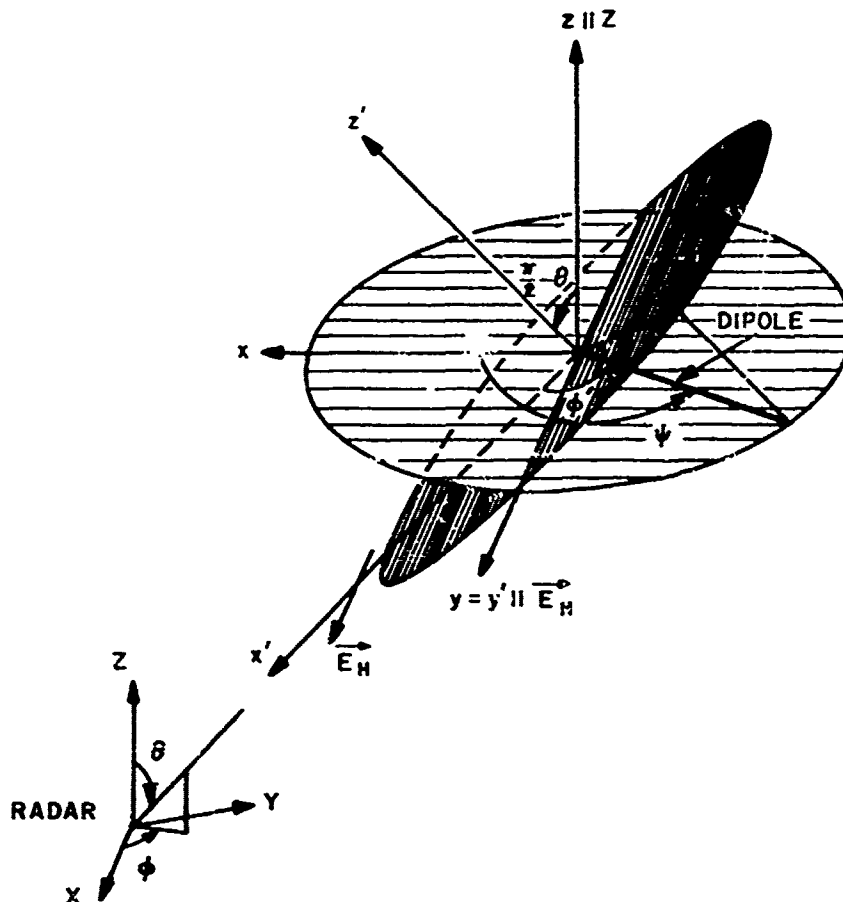


Figure 6. Geometry for horizontal polarization calculations.

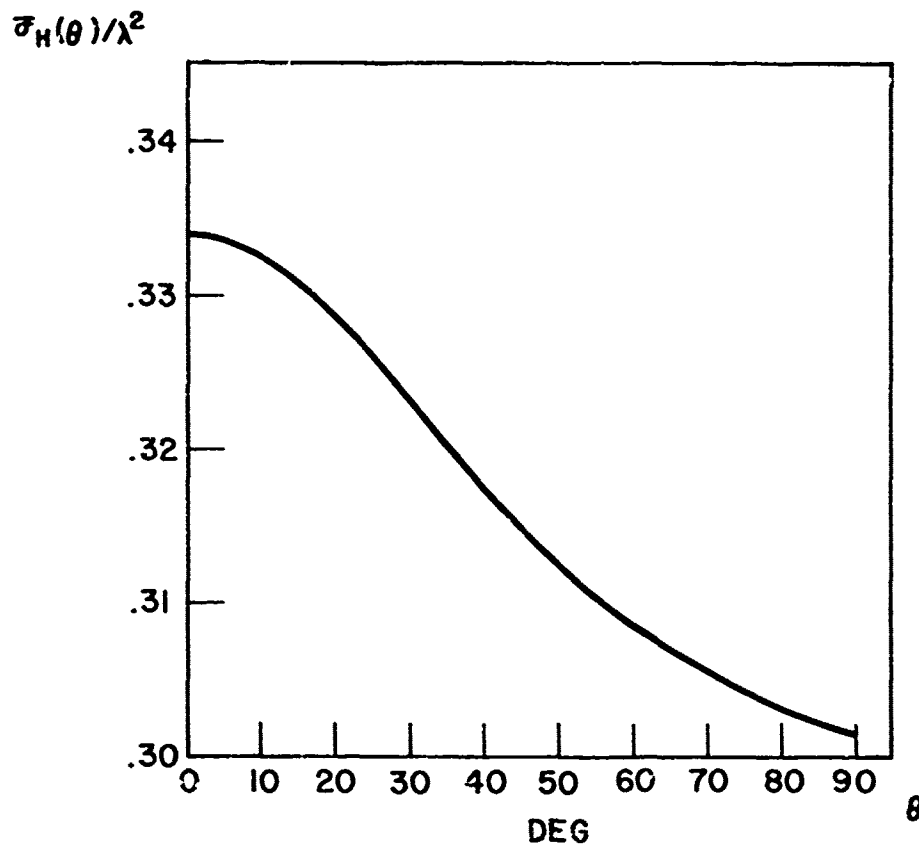


Figure 8. Mean backscatter cross section as a function of elevation (θ) of incident wave-horizontal polarization.

When the incident field is vertically polarized, the random variable Ψ may be seen to coincide with the dipole elevation angle θ' . Thus, we obtain

$$\begin{aligned} \frac{\bar{\sigma}_V(\theta)}{\lambda^2} &= \frac{0.89 |\cos^3 \theta|}{2\pi} \int_0^{2\pi} \sin^4 \Psi \, d\Psi \\ &= 0.334 |\cos^5 \theta| \end{aligned} \quad (13)$$

As to the actual distribution of dipole orientations, the available evidence appears to support the horizontal distribution at least for X-band dipoles.³ However, exoatmospheric dispersal, the selective weighting of dipoles to assume other attitudes, the recent seeding of dipoles, and the buffeting effect of turbulent air currents may give rise to chaff clouds better

³Palermo, C. J. and Bower, L. H., "Bistatic Scattering Cross Section of Chaff Dipoles with Application to Communications," Proceedings IEEE, Aug. 1965.

described by the uniform distribution of dipole orientations. In any event the mean radar cross sections per dipole for both the horizontal and uniform orientations are employed in subsequent calculations involving impulse and range-gated radar responses to various chaff clouds.

To consider the radar return from each of the dipoles contained within an arbitrary volume, we must first define a chaff dipole volume density. As noted previously we assume that the number of dipoles falling within any given region v is a Poisson distributed random variable, N_v . We shall parameterize N_v with respect to space coordinates - that is, define a random process in space by identifying N_v with each point $P(x_0, y_0, z_0)$ as follows. Let v_p be the region defined with respect to a Cartesian frame

$$v_p = \left\{ (x, y, z): x_0 - \frac{\Delta x}{2} \leq x \leq x_0 + \frac{\Delta x}{2}, y_0 - \frac{\Delta y}{2} \leq y \leq y_0 + \frac{\Delta y}{2}, z_0 - \frac{\Delta z}{2} \leq z \leq z_0 + \frac{\Delta z}{2} \right\}$$

and the volume encompassed by this region is

$$\Delta v = \Delta x \Delta y \Delta z$$

Now, let $N(v_p)$ be the number of dipoles contained within v_p . We assume that the mean value of $N(v_p)$, $E\{N(v_p)\}$, and the limit of the ratio of the mean value of $N(v_p)$ to the volume Δv as the volume shrinks to the point P exist and are continuous functions of the space coordinates. We define

$$m(v_p) \triangleq E\{N(v_p)\}, \quad (14)$$

and

$$\delta(P) \triangleq \lim_{\substack{\Delta x \rightarrow 0 \\ \Delta y \rightarrow 0 \\ \Delta z \rightarrow 0}} \frac{m(v_p)}{\Delta v}. \quad (15)$$

where $\delta(P)$ is the desired chaff dipole volume density. It should be noted that our definition of chaff volume density avoids the usual difficulties of attempting to take the limit of a discrete process (see, for example, Moore⁴). Although $N(v_p)$ is discrete so that $\lim_{\Delta v \rightarrow 0} N(v_p)/\Delta v$ cannot exist, this is not the case for $\lim_{\Delta v \rightarrow 0} E\{N(v_p)\}/\Delta v$.

The choice for the chaff dipole density function presents a problem. A realistic model for this function is not available; it depends on such parameters as the type of chaff used, method of dispersing, and prevailing winds. Our analysis is confined to two basic models: an exponentially increasing, semi-infinite distribution; and a unimodal distribution which initially increases to a maximum value and then gradually decreases. Constant-density surfaces in both cases are horizontal planes with the zero density plane at a distance h from the radar.

⁴Moore, R. K. and Williams, C. S., "Radar Return at Near-Vertical Incidence," Proceedings IRE, Vol. 45, 1957.

The first model, hereafter referred to as the exponential model, is defined by

$$\begin{aligned} \delta(h') &= \delta_m [1 - e^{-\alpha(h-h')}] & h \leq h' \\ &= 0 & h > h' \end{aligned}$$

where

h = distance from the radar to the chaff cloud top,

$\delta(h')$ = the chaff dipole volume density at the distance h' from the radar,

δ_m = maximum volume density,

α = a parameter related to the magnitude of the density gradient, that is

$$|\nabla \delta(h')_{h'=h}| = \alpha \delta_m.$$

It should be observed that in the limit as $\alpha \rightarrow \infty$, the normalized exponential density function, $\delta(h')/\delta_m$, becomes the Heaviside unit step function. Hence, this model also serves to describe the uniform-density chaff cloud with an infinite density gradient at $h' = h$.

The other model, hereafter referred to as the Rayleigh model because of its similarity to the Rayleigh probability density function, is defined as follows:

$$\begin{aligned} \delta(h') &= n \alpha (h' - h) \exp \left[-\frac{\alpha}{2} (h' - h)^2 \right] & h \leq h' \\ &= 0 & h > h' \end{aligned} \quad (17)$$

where

n is the total number of chaff dipoles contained in the vertical column with a unit cross-sectional area.

α is a parameter related to the density gradient and maximum volume density δ_m by the relationships

$$|\nabla \delta(h')_{h'=h}| = n \alpha \quad (18)$$

$$\delta_m = \delta(h') \Big|_{h'=h+1/\sqrt{\alpha}} = n \sqrt{\frac{\pi}{e}} \quad (19)$$

An important limiting case for this model is obtained again by allowing $\alpha \rightarrow \infty$. The result in this case is the Dirac delta function with intensity n . Hence, this model in the limit describes a surface layer of dipoles.

Although both models as detailed above are assumed to have infinite extent along the horizontal, such an assumption is not critical to the analysis to follow. In reality, no chaff cloud possesses either the uniformity or the infinite extent of the models postulated. It is a simple matter to eliminate the infinite extent criterion by merely cutting off the cloud at some distance from the radar greater than the maximum range cell incorporated in the radar under consideration. Whenever the chaff cloud has dimensions that are large relative to that range, the cloud's effect on the radar will be essentially as modelled. Regarding the criterion of horizontal uniformity, here again we are concerned from a practical standpoint with uniformity over that region seen by the radar. If the extent of the cloud is large relative to the observed region, then the nonuniformity due to tailing off along the periphery can be discounted.

From a computational standpoint, the use of the Rayleigh model is particularly convenient. The parameter n alone determines the number of dipoles contained in the chaff cloud. Thus, α could be allowed to change as the cloud evolves, but so long as n is constant the total number of dipoles remains constant. No such conservation rule is applicable to the exponential model with the possible exception of the infinite depth cloud, in which case an unlimited number of dipoles is involved.

As noted, α relates to the density gradient and the dispersion of the chaff cloud. It therefore constitutes an inverse age description for the cloud. Thus, α will be large immediately after dispersal (high maximum density gradient) and will decrease as the cloud settles (lower maximum density gradient). Since α is also related to the location of peak density in the Rayleigh model, the value at any given time τ after dispersal may be determined from the approximation

$$\alpha = (v_{CH} \tau)^{-2}, \quad (20)$$

where v_{CH} is the mean fall rate for the chaff dipoles.

The fact that α may be a function of time introduces nonstationarity and consequently non-ergodicity. We shall, however, be concerned with the properties of the chaff cloud during measurement intervals that are very short when compared with the reciprocal of the time derivative of $\ln \alpha$. On this basis, we shall assume that the process is quasi-stationary in the sense that its statistical properties are essentially invariant during the measurement intervals.

This paper disregards two effects common to volume-distributed scatterers: multiple scattering and shadowing. Since both effects become important in dense distributions, we shall establish a simple criterion for the degree of rarity of scatterers such that both effects are negligible. Multiple scattering arises as a consequence of the fact that the reradiated field from each dipole is a linear superposition of reradiation of the primary incident field as well as reradiation of the fields scattered by surrounding dipoles. Shadowing occurs when the primary field is attenuated in passing through intervening layers of scatterers before illuminating the deeper layers of dipoles. Both of these effects become prominent if the totality of the scattered fields is of the same order of magnitude as the primary field. If such is not the case that is, if the primary field predominates throughout the scattering region then quite obviously multiple scattering can be disregarded. Further, if little energy is removed from the primary field and reradiated as a scattered field (and little energy is dissipated thermally within the scatterers), then the attenuation due to the presence of the scatterers of the primary field as it traverses the scattering region may be neglected.

Since the fraction of the energy removed from the primary field and backscattered toward the radar is a good indication for randomly oriented scatterers of the relative magnitude of the

primary and scattered fields, we can obtain an upper limit on this ratio by considering the sum of scatterer effective cross sections. That is, we can formulate our criterion by requiring that the sum of the solid angles subtended by the scatterer cross sections be small over any angular region considered. Hence, we obtain the requirement

$$\frac{\int_{\theta_0}^{\theta_0+\Delta\theta} \int_{\phi_0}^{\phi_0+\Delta\phi} \int_{R_0}^{R_m} \frac{\bar{\sigma} \delta(r, \theta, \phi)}{4\pi r^2} r^2 \sin\theta \, dr \, d\phi \, d\theta}{\int_{\theta_0}^{\theta_0+\Delta\theta} \int_{\phi_0}^{\phi_0+\Delta\phi} \sin\theta \, d\theta \, d\phi} \ll 1, \quad (21)$$

where

R_m is the maximum distance range cell;

R_0 is the minimum distance from the radar to the scatterers; angular intervals $(\theta_0, \theta_0 + \Delta\theta)$ and $(\phi_0, \phi_0 + \Delta\phi)$ are arbitrary.

By considering angular intervals sufficiently small and applying the mean value theorem, we obtain the requirement

$$\frac{\bar{\sigma}}{4\pi} \int_{R_0}^{R_m} \delta(r, \theta_0, \phi_0) \, dr \ll 1 \quad (22)$$

If $\delta(r, \theta, \phi)$ is monotonic increasing and equation (22) holds along the direction of steepest ascent — that is, the direction determined by $\nabla\delta$ — then the inequality holds everywhere. Therefore, if multiple scattering and shadowing may be disregarded along the gradient, they may be disregarded everywhere.

For a nonmonotonic density such as the Rayleigh cloud, this criterion can be used to examine the relevance of multiple scattering and shadowing in the vertical direction for $R_m = \infty$. Inserting equation (17) into equation (22) and integrating, we obtain the results

$$\bar{\sigma} n / 4\pi \ll 1 \quad h \geq R_0, \quad (23a)$$

$$\bar{\sigma} n e^{-\alpha/2 (R_0-h)^2} / 4\pi \ll 1 \quad R_0 > h \geq 0, \quad (23b)$$

$$\bar{\sigma} n e^{-\alpha/2 R_0^2} / 4\pi \ll 1 \quad h < 0. \quad (23c)$$

Taking $\bar{\sigma} = 0.33 \lambda^2$ and using criterion (23a), we have

$$n \ll 37.74 / \lambda^2. \quad (24)$$

Considering X-band dipoles ($\lambda \approx .05$ m), we find the result

$$n < < 15,000/m^2 \quad (25)$$

as a sufficient condition for disregarding multiple scattering and shadowing effects along the vertical. Recognizing that n is the number of dipoles over a square meter, we see that such effects usually are totally negligible.

4. MEAN IMPULSE RESPONSE

4.1 Signal Return from a Single Scatterer

We consider first a radar transmitting a pulse $P_t(t)$ toward a target with radar cross section σ and located at a distance d from the radar. The backscattered received power is then given by

$$P_r(t) = P_t \left(t - \frac{2d}{c} \right) \frac{\sigma G_t G_r \lambda^2}{(4\pi)^3 d^4}, \quad t \geq \frac{2d}{c}$$

$$= 0 \quad t < \frac{2d}{c} \quad (26)$$

where G_t and G_r are the gains in the target direction of the transmitting and receiving antennas, respectively; d is the distance from the radar to the scatterer; and c is the speed of light. For simplicity we shall assume that $G_t = G_r = G$; hence, $G_t G_r = G^2$.

Strictly speaking, equation (26) is correct only for continuous wave transmission, since the width of the frequency spectrum is nonzero in every other case, and therefore the wavelength λ is not a constant. In addition the radar cross section and antenna gains are also functions of the wavelength. Nonetheless, whenever the spectrum of the transmitted pulse is narrow band, this equation provides a valid approximation to the backscattered power if we insert for λ the wavelength corresponding to the center frequency.

If the target considered is randomly oriented, the received power is also random. We find its mean value by taking the expectation of equation (26) to obtain

$$\bar{P}_r(t) = P_t \left(t - \frac{2d}{c} \right) \frac{\bar{\sigma} G^2 \lambda^2}{(4\pi)^3 d^4}, \quad t \geq \frac{2d}{c}$$

$$= 0, \quad t < \frac{2d}{c} \quad (27)$$

4.2 Signal Return from Volume Distributed Scatterers

We assume, as stated previously, that the individual scatterer locations are statistically independent. Further, we shall assume that the volume to be considered has a depth in range that is large relative to the wavelength, and that the scatterer volume density is nearly

constant over a distance large relative to the wavelength. Under these constraints, the coherent return from the volume will be entirely negligible when compared with the incoherent return.⁵ We shall therefore concentrate on the incoherent return only.

Employing the dipole volume density function defined previously, we now define a chaff volume cross section, σ_{η}^0 ,

$$\sigma_{\eta}^0(r, \theta, \phi) = \bar{\sigma}_{\eta} \delta(r, \theta, \phi), \quad (28)$$

where the subscript η refers to the common transmit and receive polarization state. (Although no major modification is required, we shall not treat cross-polarized transmission-reception states in this report.)

We shall consider the signal return from a volume ΔV , containing, by hypothesis, $N(\Delta V)$ individual dipoles. As before, $N(\Delta V)$ is a Poisson distributed random process. The incoherent radar backscatter from such a volume is obtained by summing the contribution of each scatterer contained in the incremental volume. If the incremental volume subtends a small angular sector so that the antenna gain may be considered constant across the sector, the back-scattered power is

$$\Delta P_r(t) = \frac{G^2(\theta, \phi) \lambda^2}{(4\pi)^3} \sum_{i=1}^{N(\Delta V)} P_t \left(t - \frac{d_i}{c} \right) \frac{\sigma_i}{d_i^4}, \quad (29)$$

where d_i is the distance from the radar to the i^{th} scatterer. We assume that the dimensions of the incremental volume are small relative to the mean distance to the radar; that is $d_i \gg \sqrt[3]{\Delta V}$, then

$$\Delta P_r(t) = \frac{G^2 \lambda^2 P_t \left(t - \frac{2d}{c} \right)}{(4\pi)^3 d^4} \sum_{i=1}^{N(\Delta V)} \sigma_i, \quad (30)$$

where explicit dependence on the angles θ and ϕ has been suppressed. Assuming the σ_i to be distributed with mean $\bar{\sigma}_{\eta}$ and with $m(\Delta V)$ as the mean value of $N(\Delta V)$, we obtain for the expected value of $\Delta P_r(t)$

$$\overline{\Delta P_r(t)} = \frac{G^2 \lambda^2 P_t \left(t - \frac{2d}{c} \right)}{(4\pi)^3 d^4} m(\Delta V) \bar{\sigma}_{\eta} \quad (31)$$

⁵Siegert, A. and Goldstein, H., "Coherent and Incoherent Scattering from Assemblies of Scatterers," in Propagation of Short Radio Waves, Kerr, D. E., ed., McGraw-Hill, New York, 1951.

Dividing both sides by ΔV , taking the limit as ΔV shrinks to the point (d, θ, ϕ) and using equation (15), we obtain

$$\frac{d\bar{P}}{dV}(t) = \frac{G^2 \lambda^2 P_t \left(t - \frac{2d}{c} \right)}{(4\pi)^3 d^4} \delta(d, \theta, \phi) \bar{\sigma}_\eta \quad (32)$$

Substituting equation (28), we have

$$\frac{d\bar{P}_r}{dV}(t) = \frac{G^2 \lambda^2 P_t \left(t - \frac{2d}{c} \right)}{(4\pi)^3 d^4} \sigma_\eta^0(d, \theta, \phi) \quad (33)$$

The mean received power scattered from an arbitrary volume V is then given by

$$\bar{P}_r(t) = \frac{\lambda^2}{(4\pi)^3} \int_V P_t \left(t - \frac{2d}{c} \right) \frac{\sigma_\eta^0 G^2}{d^4} dV \quad (34)$$

where σ_η^0 and G are functions of location and aspect, respectively. Equation (34) is a general expression for the mean backscatter from chaff but is not especially useful in its present form. To carry the analysis further, we shall reduce this expression to a more tractable form, but let us first clarify the use of equation (34) by considering several specific examples.

4.2.1 Scattering from a Semi-Infinite Cloud

Consider the geometry shown in figure 9. An isotropic antenna of gain G is located at a height h above the chaff cloud which has uniform density and unbounded depth. A spherical coordinate system with its origin at the radar is used. In such a case, equation (34) becomes

$$\bar{P}_r(t) = \frac{G^2 \sigma_\eta^0 \lambda^2}{(4\pi)^3} \int_h^\infty \int_0^\pi \int_0^{2\pi} \frac{P_t \left(t - \frac{2r}{c} \right)}{r^4} r^2 \sin \theta d\phi d\theta dr \quad (35)$$

where $\theta = \cos^{-1}(-h/r)$ and we have assumed a constant σ_η^0 so that it has been removed from the integral. Integrating equation (35) in ϕ and θ , we have

$$\bar{P}_r(t) = \frac{G^2 \sigma_\eta^0 \lambda^2}{2(4\pi)^2} \int_h^\infty P_t \left(t - \frac{2r}{c} \right) \left[\frac{1}{r^2} - \frac{h}{r^3} \right] dr \quad (36)$$

Introducing a change of variables $2r/c = \tau$, and using the fact that $P_t(t - 2r/c) = 0$ for $t \leq 2r/c$, we obtain

$$\bar{P}_r(t) = \frac{G^2 \sigma_\eta^0 \lambda^2}{(4\pi)^2 c} \int_{2h/c}^t P_t(t - \tau) \left[\frac{1}{\tau^2} - \frac{2h}{c} \frac{1}{\tau^3} \right] d\tau \quad (37)$$

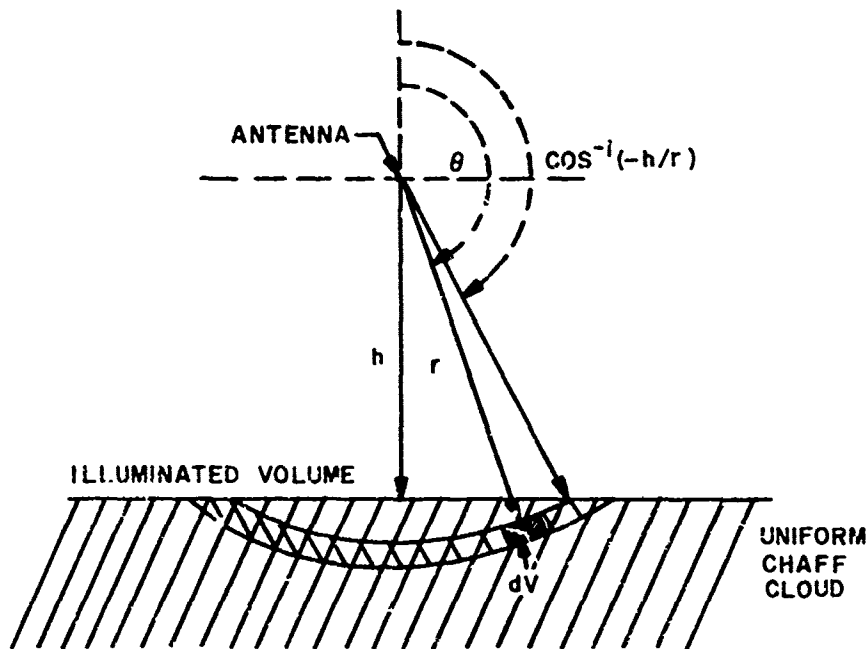


Figure 9. Cross section of a semi-infinite chaff cloud.

Equation (37) can now be recognized as a superposition integral with $P_t(t)$ as the driving function and

$$P_r^{\delta}(t) = \frac{G^2 \lambda^2 \sigma_{\eta}^0}{(4\pi)^2 c} \left[\frac{1}{t^2} - \frac{2h}{c} \frac{1}{t^3} \right], \quad t > \frac{2h}{c} \quad (38)$$

$$= 0, \quad t \leq \frac{2h}{c}$$

as the response to an impulse function. We should note that equation (38) is not formally correct, since by postulating an impulsive transmitted waveform we have violated our premise on the extent of the illuminated region. However, the impulse response function does provide a valuable tool, since a solution may be obtained by convolving the impulse response with any transmitted waveform that has sufficient spatial extent so that this premise is not violated. Further, convolution with a transmitted waveform with a spatial extent of several wavelengths will not, in general, provide a result significantly different from the impulse response function. Hence, we may consider the impulse response function as an approximate solution to the chaff backscatter problem whenever the transmitted pulse has a duration very short as compared with the impulse response but a spatial extent of at least several wavelengths.

If we introduce another variable $d = ct/2$, which may be interpreted as the distance from which the signal is arriving at time t , we have

$$P_r^\delta(t) = \left[\frac{G^2 \lambda^2}{(4\pi)^2} \right] \left[\frac{\sigma_\eta^0}{c t^2} \left(1 - \frac{h}{d} \right) \right], \quad \frac{h}{d} < 1$$

$$= 0, \quad \frac{h}{d} \geq 1. \quad (39)$$

Note that the first part of this equation is a function of physical parameters, and the second part is a function of time and specifies the shape of the returned pulse.

4.2.2 Finite Thickness Chaff Layers

The return for a finite thickness uniform density chaff cloud follows directly from equation (39). If the upper edge of the chaff layer is at h_1 and the lower edge at h_2 , then

$$P_r^\delta(t) = 0, \quad \frac{h_1}{d} > 1 \quad (40a)$$

$$P_r^\delta(t) = \frac{G^2 \lambda^2 \sigma_\eta^0}{(4\pi)^2} \frac{1}{c t^2} \left(1 - \frac{h_1}{d} \right), \quad \frac{h_1}{d} < 1 \quad (40b)$$

$$P_r^\delta(t) = \frac{G^2 \lambda^2 \sigma_\eta^0}{(4\pi)^2} \left[\frac{1}{c t^2} \left(1 - \frac{h_1}{d} \right) - \left(1 - \frac{h_2}{d} \right) \right]$$

$$= \frac{G^2 \lambda^2 \sigma_\eta^0}{(4\pi)^2} \frac{1}{c t^2} \left[\frac{h_2}{d} - \frac{h_1}{d} \right], \quad \frac{h_2}{d} < 1. \quad (40c)$$

There is the regular range delay until the pulse hits the cloud. Then before the pulse reaches the trailing edge at h_2 , the return is the same as that from a semi-infinite cloud; and after the leading edge of the pulse has passed through the chaff layer, the return is given by equation (40c).

4.2.3 Varying Density Chaff

We can find the differential power return from a chaff layer of infinitesimal thickness by allowing $(h_2 - h_1)$, equation (40c), to shrink to dh giving

$$dP_r^\delta(t) = \frac{G^2 \lambda^2}{(4\pi)^2} \frac{\sigma_\eta^0}{c t^2} \frac{1}{d} dh. \quad (41)$$

The volume cross section σ_η^0 , which up to now has been treated as a constant, can now be treated as a variable when we integrate both sides of equation (41). The returned power from a varying density chaff cloud is then

$$P_r^\delta(t) = \frac{G^2 \lambda^2}{(4\pi)^2} \frac{1}{c} \frac{1}{t^2} \int_0^d \sigma_\eta^0(h) dh. \quad (42)$$

Having examined some simple examples and introduced the concept of the chaff impulse response, let us return to the more general form of equation (34). We note that for those dipole orientation distributions considered in section 3, $\bar{\sigma}_\eta$ has the form $\lambda^2 C_\eta |\cos \theta|^{k(\eta)}$. (In the horizontally polarized, horizontally distributed case we may use the approximation $\sigma_\eta^h = 0.32\lambda^2$.) We shall consider hypothetical antenna gain functions of the form $G(\theta) = G_0^h |\cos \theta|^\ell$. Equation (34) becomes

$$\bar{P}_r(t) = \frac{G_0^2 C_\eta \lambda^4}{(4\pi)^3} \int_{h_m}^\infty \int_\theta^\pi \int_0^{2\pi} \frac{P_t \left(t - \frac{2r}{c}\right)}{r^2} |\cos \theta|^{2\ell+k} \sin \theta \delta(r, \theta) d\phi d\theta dr, \quad (43)$$

where

$$\begin{aligned} \delta(r, \theta) &= \delta_m \{1 - \exp[-\alpha r (\cos \theta - \cos \theta)]\}, & \theta \geq \theta \\ &= 0, & \theta < \theta \end{aligned} \quad (44)$$

for the exponential chaff model, and

$$\begin{aligned} \delta(r, \theta) &= n \alpha r (\cos \theta - \cos \theta) \exp\left[-\frac{\alpha r^2}{2} (\cos \theta - \cos \theta)\right], & \theta \geq \theta \\ &= 0, & \theta < \theta \end{aligned} \quad (45)$$

for the Rayleigh chaff model, with

$$\theta = \begin{cases} 0 & |h/r| > 1 \\ \cos^{-1}(-h/r) & |h/r| < 1, \text{ and} \end{cases}$$

$h_m = \max(0, h)$.

Integrating with respect to ϕ and using an impulse driving function, we have

$$P_r^\delta(t) = \frac{c G_0^2 \lambda^4 C_\eta}{4 (4\pi)^2} \left(\frac{2}{c t}\right)^2 \int_\theta^\pi |\cos \theta|^{2\ell+k} \sin \theta \delta\left(\frac{c t}{2}, \theta\right) d\theta. \quad (46)$$

Returning to our previous notation, that is, $h' = -ct/2 \cos \theta$, we obtain

$$P_r^\delta(t) = \frac{c G_0^2 \lambda^4 C_\eta}{4 (4\pi)^2} \left(\frac{2}{c t}\right)^{2\ell+k+3} \int_{d_m}^{ct/2} |h'|^{2\ell+k} \delta(h, h') dh', \quad (47)$$

where $d_m = \max(h, -ct/2)$. Substituting $d = ct/2$ and defining $R(\lambda, \eta) = cG_0^2 \lambda^4 C_\eta / 4(4\pi)$, we obtain

$$P_r^\delta(d) = \frac{R(\lambda, \eta)}{d^{2\ell+k+3}} \left[\int_0^d h'^{k+2\ell} \delta(h, h') dh - (\text{sgn } d_m)^k \int_0^{d_m} h'^{k+2\ell} \delta(h, h') dh' \right] \quad (48)$$

where

$$\text{sgn } d_m = \begin{cases} 1 & \text{for } d_m > 0 \\ -1 & \text{for } d_m < 0 \end{cases}$$

Upon substituting for the exponentially varying chaff density, we obtain an integral that can be reduced by successive integration by parts with the following result:

$$\int_0^d h'^s (1 - e^{-\alpha(h'-h)}) dh' = \frac{d^{s+1}}{s+1} + \frac{s! e^{\alpha h}}{\alpha^{s+1}} + e^{-\alpha(d-h)} \sum_{i=0}^s \frac{s!}{i!} \frac{d^i}{\alpha^{s-i+1}} \quad (49)$$

A similar application of successive integration by parts results in an iterative solution when the Rayleigh chaff density is substituted. If we define

$$I(s) = \int_0^d h'^s (h' - h) e^{-\alpha/2 (h' - h)^2} dh', \quad (50)$$

we obtain the iterative formula

$$I(s) = L_s + s h^{s-1} \phi + \frac{s}{\alpha} \sum_{i=0}^{s-2} h^i I(s-i-2), \quad (51)$$

where

$$\begin{aligned} L_s &= e^{-\alpha h^2/2} - e^{-\alpha/2 (d-h)^2} = I(0), & s &= 0 \\ &= -d^s e^{-\alpha/2 (d-h)^2}, & s &= 1, 2, \dots \end{aligned}$$

$$\begin{aligned} \phi &= \int_0^d e^{-\alpha/2 (h'-h)^2} dh' \\ &= \sqrt{\frac{\pi}{2\alpha}} \left\{ \text{erf} \left[\sqrt{\frac{\alpha}{2}} (d-h) \right] + \text{erf} \left[\sqrt{\frac{\alpha}{2}} h \right] \right\}. \end{aligned}$$

We shall exemplify the use of these formulas by considering four hypothetical antenna patterns: an isotropic pattern, two teardrop lobe structures, and a hollow cone pattern which may be represented, respectively, as

$$G_1^2 = G_{10}^2 \quad \text{isotropic pattern;} \quad (52)$$

$$G_2^2 = G_{20}^2 \cos^4(\theta) \quad 0 \leq \theta \leq \pi, \quad \text{double-lobe;} \quad (53)$$

$$G_3^2 = G_{30}^2 \cos^4 \theta \quad \frac{\pi}{2} \leq \theta \leq \pi \quad \text{single-lobe;} \quad (54)$$

$$0 \leq \theta < \frac{\pi}{2}$$

$$G_4^2 = 4 G_{40}^2 (1 - \cos^2 \theta) \cos^2 \theta \quad \frac{\pi}{2} \leq \theta \leq \pi \quad \text{hollow cone,} \quad (55)$$

$$= 0 \quad 0 \leq \theta < \frac{\pi}{2}$$

where G_{10} , G_{20} , G_{30} , and G_{40} are the peak power gains of the assumed antennas.

We obtain the chaff impulse response for a radar system employing these antenna when both exponential and Rayleigh cloud models are considered and the chaff dipoles are uniformly oriented for both polarization states, or the dipoles are horizontally distributed and the transmission-reception polarization is horizontal. We also consider the combination of an isotropic antenna, horizontally distributed chaff orientations and a vertically polarized wave. The specific impulse response functions obtained in each case are enumerated in appendix A. The results are also plotted as figures 10 through 17.

It should be observed that the impulse response functions for chaff return differ significantly from those obtained from ground return.⁶ While the impulsive response from surface-distributed scatterers obtains its maximum value initially, the impulsive response from chaff rises to its peak value only after the incident wave has penetrated some non-zero depth into the scatter volume. The amount of retardation of peak return relative to initial return depends upon the distance from the radar to the chaff cloud and the specific model considered. In general, the impulse response for chaff peaks most rapidly when the radar antenna is narrow-beam and the magnitude of the chaff cloud density gradient is large. It may further be observed that when the chaff dipoles assume a horizontal orientation and the polarization is vertical, the net effect on the impulse response is equivalent to the effect obtained by using a narrower beam antenna; that is, backscatter from the vertical direction is accentuated whereas returns from lateral directions are strongly attenuated. Thus, a horizontal orientation of dipoles with vertical polarization increases the rapidity with which the impulse response peaks, with the consequence that the chaff cloud response more closely resembles the surface scattering of rough terrain.

Of perhaps even greater importance than the chaff impulse response is the chaff range-gated response that is, the return to the radar from a specific range resolution cell extending from d to $d + \Delta d$ as the radar altitude h is allowed to vary.

The mean power return from chaff at time, t , is given by the convolution of the transmitted pulse, P_t , with the mean impulse response

⁶Edison, A. R., Moore, R. K., and Warner, B. D., "Radar Return at Near-Vertical Incidence, Summary Report," Univ. of New Mexico Engineering Experiment Station, Tech. Rep. EE-24, Sept. 1959.

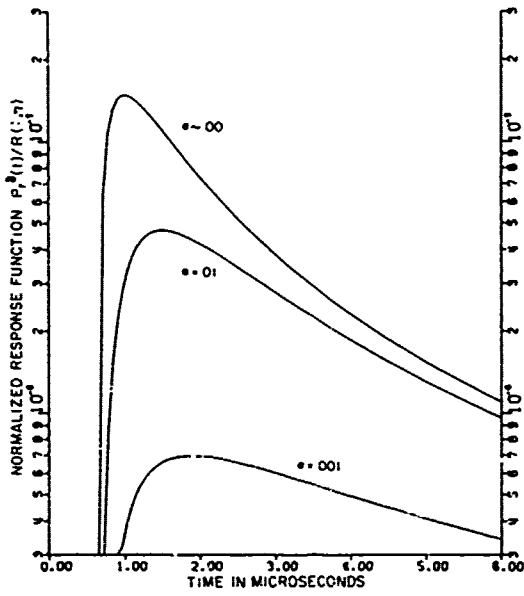


Figure 10. Impulse response functions at $h = 100$ m for an isotropic antenna pattern and uniformly distributed dipole orientations (exponential cloud model)

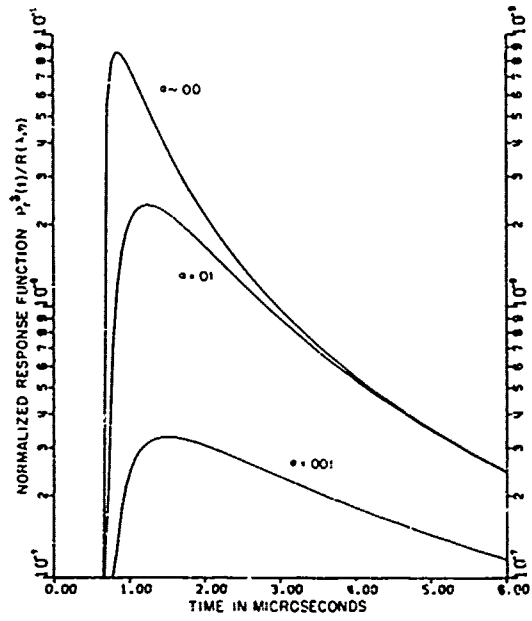


Figure 11. Impulse response functions at $h = 100$ m for a $\cos^2 \theta$ antenna pattern and uniformly distributed dipole orientations (exponential cloud model)

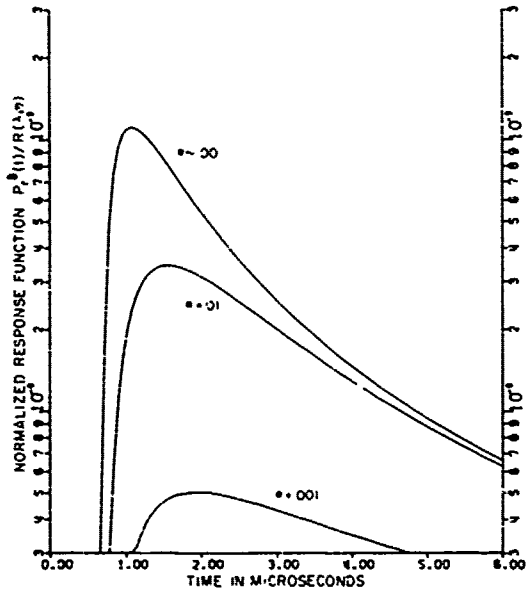


Figure 12. Impulse response functions at $h = 100$ m for a $\sin \theta \cos \theta$ antenna pattern and uniformly distributed dipole orientations (exponential cloud model)

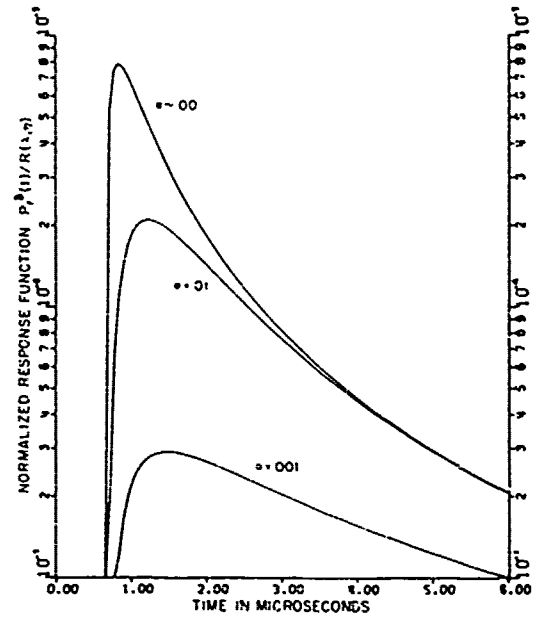


Figure 13. Impulse response functions at $h = 100$ m for an isotropic antenna pattern, vertically polarized wave, and horizontally distributed dipole orientations (exponential cloud model)

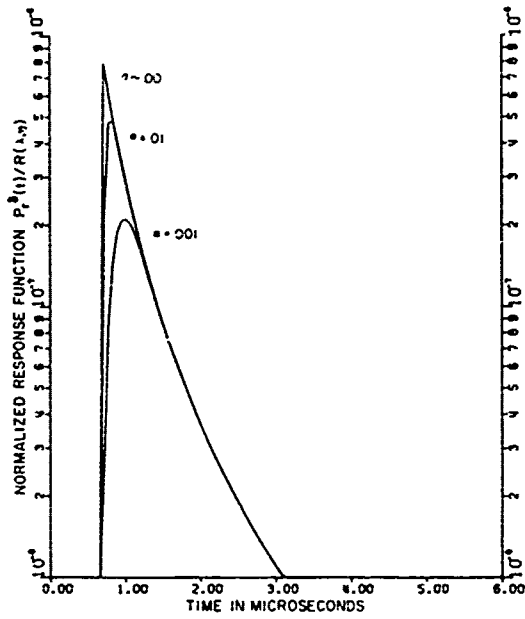


Figure 14. Impulse response functions at $h = 100$ m for an isotropic antenna pattern and uniformly distributed dipole orientations (Rayleigh cloud model)

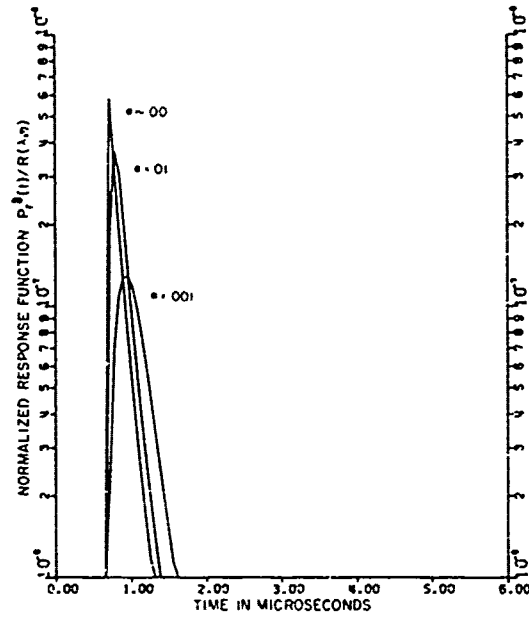


Figure 15. Impulse response functions at $h = 100$ m for a $\cos^2\theta$ antenna pattern and uniformly distributed dipole orientations (Rayleigh cloud model)

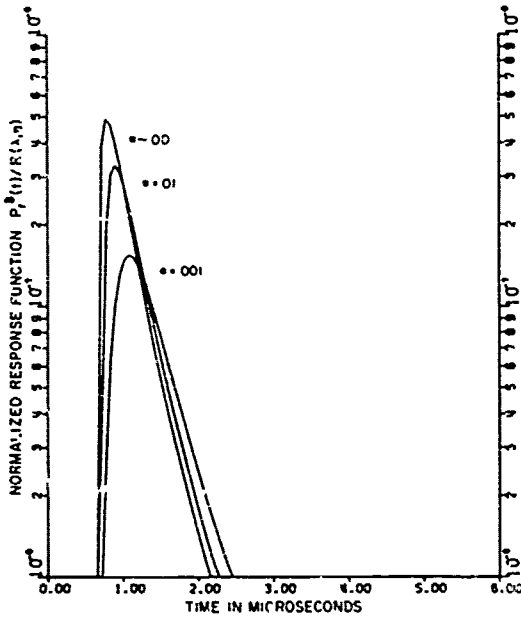


Figure 16. Impulse response functions at $h = 100$ m for a $\sin\theta\cos\theta$ antenna pattern and uniformly distributed dipole orientations (Rayleigh cloud model)

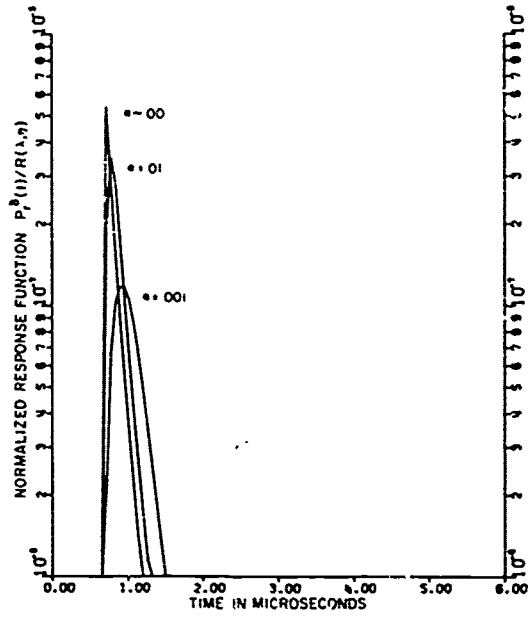


Figure 17. Impulse response functions at $h = 100$ m for an isotropic antenna pattern, vertically polarized wave, and horizontally distributed dipole orientations (Rayleigh cloud model)

$$\bar{P}_r(t) = \int_h^{ct/2} P_t \left(t - \frac{2r}{c} \right) P_r^\delta(r) dr. \quad (56)$$

If the transmitted wave amplitude is constant with $P_t(t) = P_0$, and we are concerned only with the return contributed by dipoles lying at ranges between d and $d + \Delta d$ from the radar, we obtain for $d \geq h$

$$\overline{\Delta P}_r(d) = \int_d^{d+\Delta d} P_0 P_r^\delta(r) dr, \quad (57)$$

which becomes, for Δd , sufficiently short

$$\overline{\Delta P}_r(d) = \Delta d P_0 P_r^\delta(d). \quad (58)$$

When rewritten as the ratio

$$\overline{\Delta P}_r(d)/P_0 = \Delta d P_r^\delta(d), \quad (59)$$

we obtain the chaff backscatter loop attenuation for the range cell $(d, d + \Delta d)$.

Considering the hypothetical antenna patterns and dipole orientations previously introduced, we have plotted representative chaff backscatter loop attenuation functions versus radar altitude as figures 18 through 27.

5. PROBABILITY DENSITY FUNCTIONS FOR CHAFF BACKSCATTER

Since, by hypothesis, the chaff dipoles are randomly and independently distributed and randomly oriented, the statistics of the scattered field are identical with those for the sum of sine waves with random identically distributed amplitudes and phases. It is well known that such a process is asymptotically Gaussian when the number of constituent waves of the sum is large.⁷ The envelope of a Gaussian process will be Rayleigh distributed when it is defined for narrow-band processes in the manner of Rice⁷ and when the broader definition of envelope as the absolute value of the complex-valued function obtained by adding to the given function i times its Hilbert transform is used. Thus, we should expect that the envelope of the chaff return process will be Rayleigh distributed and that the amplitude of the squared and low-pass filtered return will be exponentially distributed for a sufficiently large number of chaff dipoles contributing to the return.⁸ Hence, the radar cross section for chaff which is proportional to the backscattered power should have a probability distribution which is asymptotically exponential as the number of contributing dipoles becomes large.

⁷Rice, S., "Mathematical Analysis of Random Noise," Bell Systems Technical Journal, vol. 23, 1944 and vol. 24, 1945.

⁸Borison, S. L., "Statistics of the Radar Cross Section of a Volume of Chaff," MIT, Lincoln Laboratory, Group Rep 1965-10, 1965.

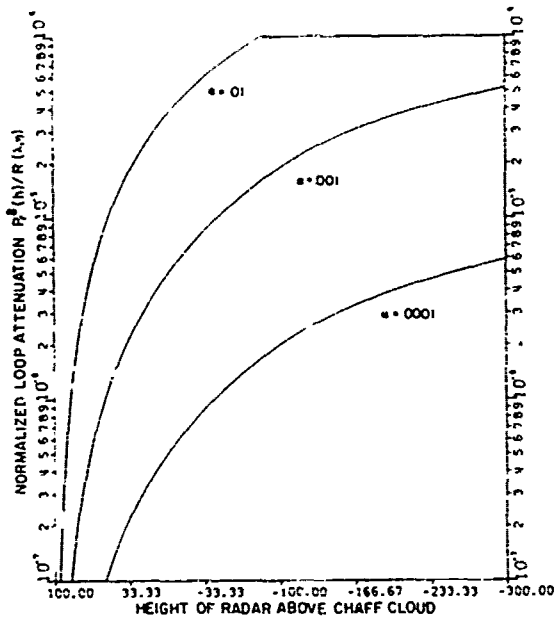


Figure 18. Range-gated response at $d = 100$ m for an isotropic antenna pattern and uniformly distributed dipole orientations (exponential cloud model)

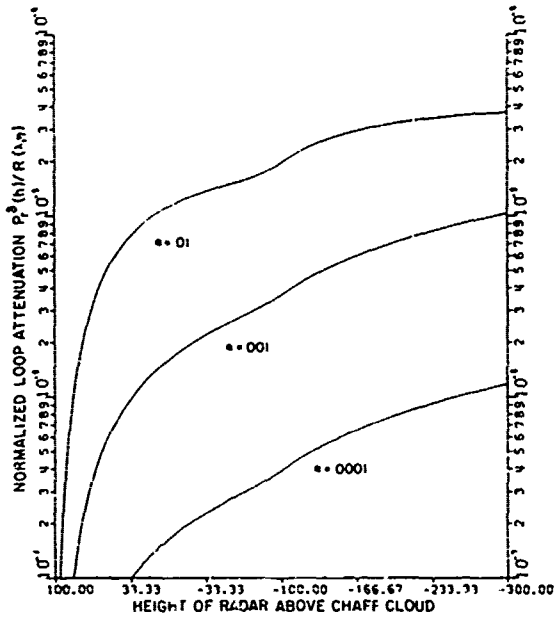


Figure 19. Range-gated response at $d = 100$ m for a $\cos^2\theta$ antenna pattern and uniformly distributed dipole orientations (exponential cloud model)

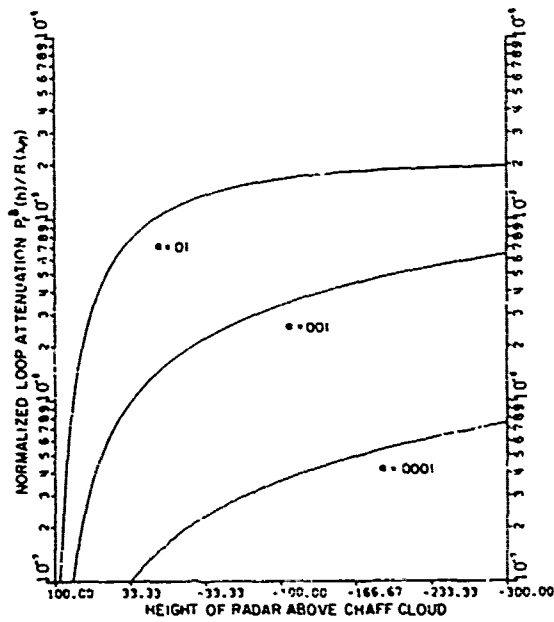


Figure 20. Range-gated response at $d = 100$ m for a single-lobe $\cos^2\theta$ antenna pattern and uniformly distributed dipole orientations (exponential cloud model)

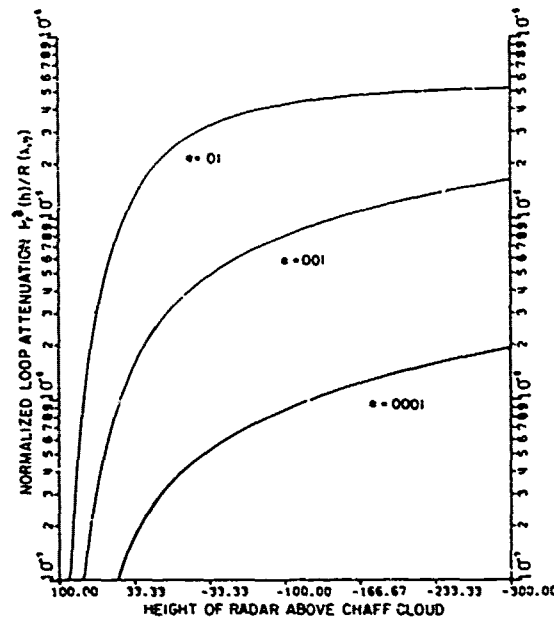


Figure 21. Range-gated response at $d = 100$ m for a $\sin\theta\cos\theta$ antenna pattern and uniformly distributed dipole orientations (exponential cloud model)

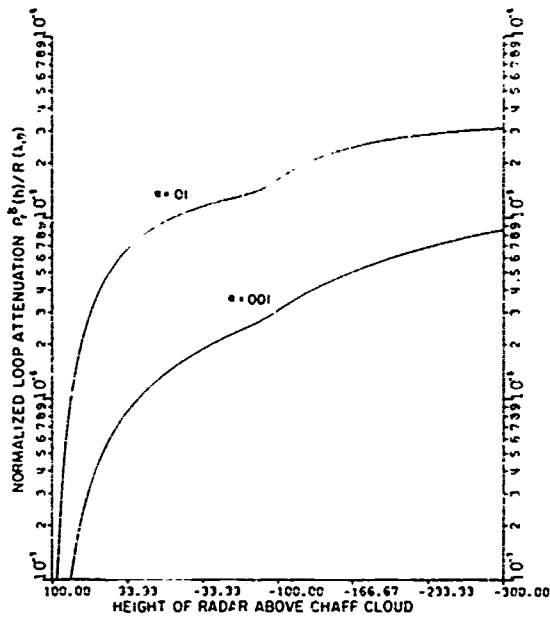


Figure 22. Range-gated response at $d = 100$ m for an isotropic antenna pattern, vertically polarized wave, and horizontally distributed dipole orientations (exponential cloud model)

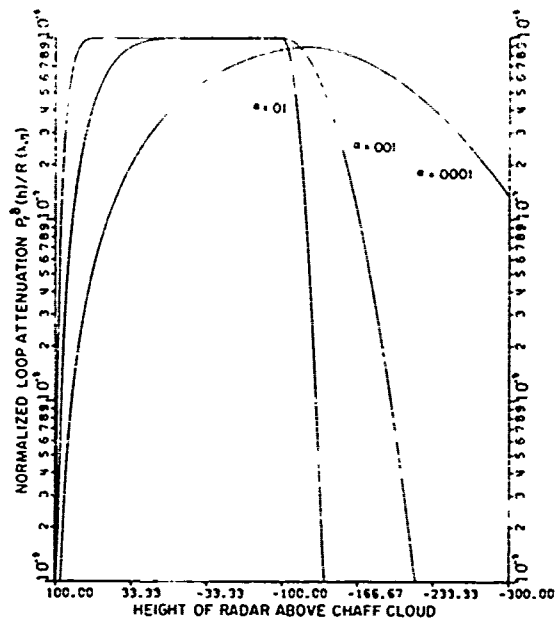


Figure 23. Range-gated response at $d = 100$ m for an isotropic antenna pattern and uniformly distributed dipole orientations (Rayleigh cloud model)

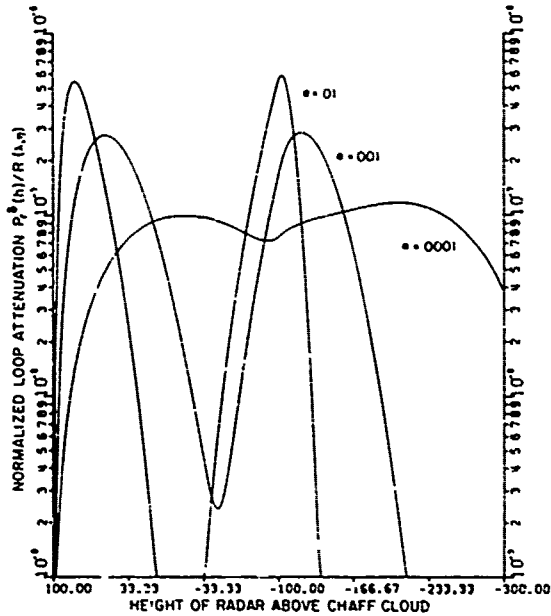


Figure 24. Range-gated response at $d = 100$ m for a $\cos^2\theta$ antenna pattern and uniformly distributed dipole orientations (Rayleigh cloud model)

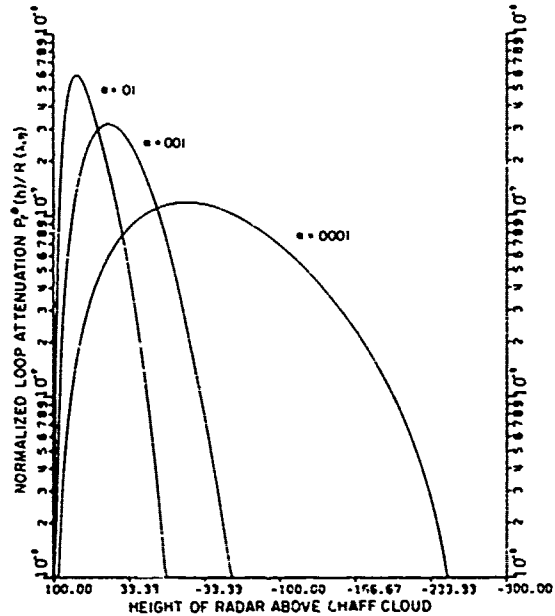


Figure 25. Range-gated response at $d = 100$ m for a single lobe $\cos^2\theta$ antenna pattern and uniformly distributed dipole orientations (Rayleigh cloud model)

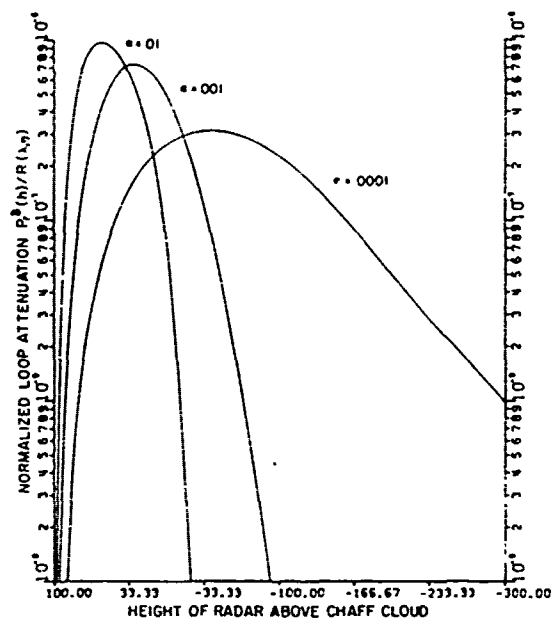


Figure 25. Range-gated response at $d = 100$ m for a $\sin\theta\cos\theta$ antenna pattern and uniformly distributed dipole orientations (Rayleigh cloud model)

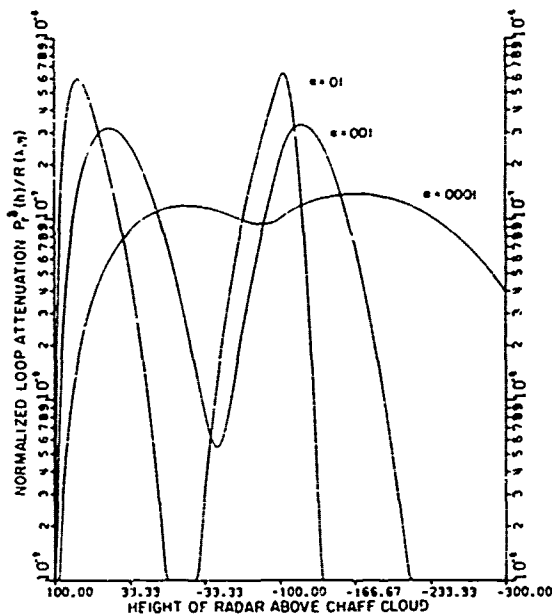


Figure 27. Range-gated response at $d = 100$ m for an isotropic antenna pattern, vertically polarized wave, and horizontally distributed dipole orientations (Rayleigh cloud model)

The fact that the instantaneous voltage variate of the return signal is Gaussian in the limit is a consequence of the central-limit theorem of probability theory and is not dependent upon the distribution of the component amplitudes of the individual dipole returns. The rate at which this limiting form is approached, however, does depend on this distribution. Goudsmit and Schiff have examined the finite number of scatterers case and have found the Gaussian distribution to be a good approximation when ranges to the contributing dipoles are all equal, even when the number of dipoles equals 4 or 5. When the number is 10 or more, they found the differences are completely negligible.⁵ Borison has also examined the use of the exponential law for describing the chaff radar cross section and concluded that the approximation is good when the average number of dipoles in the radar resolution volume is greater than two or three.⁸

Since the exponential probability law is a single parameter distribution, it is completely determined by its mean value. Thus, we may represent the first order distribution for chaff radar cross section as

$$p(\sigma_\eta) = \frac{1}{\sigma_\eta^0} e^{-\sigma_\eta/\sigma_\eta^0} \quad (60)$$

⁵Siegert, A. and Goldstein, H., "Coherent and Incoherent Scattering from Assemblies of Scatterers," in *Propagation of Short Radio Waves*, Kerr, D. E., ed., McGraw-Hill, New York, 1951.

⁸Borison, S. L., "Statistics of the Radar Cross Section of a Volume of Chaff," MIT, Lincoln Laboratory, Group Rep 1965-10, 1965.

For such a distribution, we note that the variance equals the square of the mean, and that including more dipoles in the radar resolution cell by increasing the resolution cell size does not narrow the relative distribution width, since the mean to rms ratio is constant. It should be observed that the most probable value of backscattered power is zero. The return power will be less than half the average value 29 percent of the time and greater than twice the average 14 percent of the time.

As the radar moves relative to the chaff cloud, the path lengths to the individual dipoles will vary. The doppler shifts thus introduced will, in general, be different for each dipole scatterer; hence, frequency dispersion, rather than mere frequency shift, will result in a return signal that is noise-like and narrow-band when the transmitted signal frequency is greater than the maximum doppler shift. Successive samples obtained by a pulsed radar will generally be correlated, the degree of correlation for a fixed sampling period depending on the width of the doppler dispersion spectrum.

The second order probability density for sample powers P_1 and P_2 with sampling interval τ becomes

$$P_2(P_1, P_2, \tau) = \frac{e^{-(P_1 + P_2)/P_A(1-\rho)}}{P_A^2(1-\rho)} I_0\left(\frac{2\sqrt{\rho P_1 P_2}}{P_A(1-\rho)}\right) \quad (61)$$

where P_A is the average returned power, and the correlation coefficient $\rho(\tau)$ is defined by

$$\rho(\tau) = \frac{\overline{P_1 P_2} - \bar{P}_1 \bar{P}_2}{P_A^2} \quad (62)$$

and I_0 is the zeroth order modified Bessel function of the first kind. For τ sufficiently large so that

$$\overline{P_1 P_2} - \bar{P}_1 \bar{P}_2 = P_A^2 \quad (63)$$

we observe that $\rho(\tau) \rightarrow 0$; and, as expected, we have

$$P_2(P_1, P_2; \tau) \rightarrow P(P_1) P(P_2) \quad (64)$$

That is, when the sampling interval is sufficiently long so that the correlation coefficient is zero, the sampled return powers are not only uncorrelated but also independent.

6. POWER SPECTRAL DENSITY

Of paramount importance in determining whether the return powers from successive return pulses are uncorrelated is the width of the power spectral density. The correlation of detected pulse amplitude from pulse-to-pulse affects the required integration time to achieve a given detection probability; for high detection probabilities, the greater the correlation, the longer the required integration time.

The successive range-gated pulse returns from chaff may be considered analogous to the sequence of sampled values obtained by periodically sampling a random process. As we have previously noted, each of the dipoles may be thought of as a simple harmonic generator, transmitting with random phase and amplitude and with a frequency determined by the radar transmission frequency and the doppler shift induced by its motion relative to the radar. The ensemble of returns as seen at the radar comprises a narrow-band, noise-like process, the decorrelation time of which is inversely proportional to its bandwidth. If this decorrelation time is short compared with the radar pulse repetition period, successive pulses will provide independent samples.

Although the chaff cloud drift velocity and dipole rotations are major contributors to the doppler shift for a stationary radar,⁹ these factors are not significant when compared with the frequency shift induced by the rapid movement of the airborne radar altimeter. Therefore, in calculating the power spectral density, we shall consider only the radar movement.

In calculating the chaff return power spectral density we note that the doppler frequency shift is the same for signal returns from dipoles whose position vectors' intersections with the radar velocity vector form equal angles (see fig. 1). The amount of power returned at any doppler-shifted frequency depends therefore on the antenna gain in the specified direction, and the chaff radar cross section in that direction and at the range-gate distance from the radar. The locus of points contributing to the power spectral density at any specified frequency within the doppler band describes a circle or an arc of a circle, the locus being the projection of a cone on that portion of the range gate sphere lying within the chaff cloud.

In determining the doppler power spectral density function we concern ourselves with the frequency band referenced to the transmitter frequency f_0 . If the maximum doppler shift is less than f_0 , the return signal is narrow band and two distinct bands of frequencies, one positive f_+ , the other negative f_- , are discernible. Thus, with respect to the doppler frequency variable f_D , we may write $f_{\pm} = \pm(f_0 + f_D)$.

The incremental power density due to return from an element of arc lying along the prescribed locus of points may be written

$$dP(f_D) \sim \sigma_{\eta}^0(\theta) G^2(\theta, \phi) ds, \quad (65)$$

where, in spherical coordinates,

$$ds = \sqrt{\sin^2 \theta d\phi^2 + d\theta^2}$$

The power density from the entire locus of equal doppler shifted points becomes

$$P(f_D) \sim \int_C \sigma_{\eta}^0(\theta) G^2(\theta, \phi) \sqrt{\sin^2 \theta d\phi^2 + d\theta^2}, \quad (66)$$

where C defines the path of integration.

⁹Wong, J. L., Reed, I. S., and Kaprielian, Z. A., "A Model for Radar Echoes from a Random Collection of Rotating Dipole Scatterers," USCEE Report 159, Jan. 1966.

Defining θ_0 as the angle between position vectors to the contributing dipoles and the radar velocity vector, we observe

$$\theta_0 = \cos^{-1} \left(\frac{c f_D}{2 V f_0} \right), \quad (67)$$

where

f_D is the doppler frequency shift,

f_0 is the transmitted frequency (center frequency for a narrow band signal), and

V is the magnitude of the radar velocity.

The locus of points C , defining the integration path, may be found by setting the normalized inner product of the contributing dipole position vectors and the radar velocity vector equal to $\cos \theta_0$. Hence, we obtain

$$\cos \phi = (\cos \theta_0 + \cos \theta \cos \gamma) / \sin \theta \sin \gamma, \quad (68)$$

$$d\phi = \frac{\cos \gamma + \cos \theta_0 \cos \theta}{\sin \theta} [\sin^2 \theta \sin^2 \gamma - (\cos \theta_0 + \cos \theta \cos \gamma)^2]^{-1/2} d\theta. \quad (69)$$

Inserting equation (69) in equation (65), we have

$$P(f_D) \sim \int_{\theta_0}^{\pi} \frac{\sigma_{\eta}^0(\theta) G^2(\theta, \phi) \sin \theta \sin \theta_0 d\theta}{\sqrt{\sin^2 \theta - 2 \cos \theta_0 \cos \gamma - \cos^2 \gamma - \cos^2 \theta_0}}, \quad (70)$$

where $\theta = \cos^{-1} (-h/d)$.

For $\gamma = \pi/2$, horizontal flight, this becomes

$$P(f_D) \sim \int_{\theta_0}^{\pi} \frac{\sigma_{\eta}^0(\theta) G^2(\theta, \phi) \sin \theta \sin \theta_0 d\theta}{\sqrt{\sin^2 \theta - \cos^2 \theta_0}}. \quad (71)$$

For $\gamma = 0$, vertical flight, we observe that $\pi - \theta = \theta_0$, and obtain

$$P(f_D) \sim \sigma_{\eta}^0(\pi - \theta_0) \sin \theta_0 \int_0^{2\pi} G^2(\pi - \theta_0, \phi) d\phi, \quad (72)$$

where $0 \leq \theta_0 \leq \cos^{-1} (h/d)$.

For G independent of ϕ , as in the cases previously introduced, we have

$$P(f_D) \sim \sigma_n^0 (\pi - \theta_0) \sin \theta_0 G^2 (\pi - \theta_0). \quad (73)$$

This becomes, for a uniform density chaff cloud with uniformly distributed dipole orientations, with the range gate completely submerged, and with an isotropic antenna,

$$P(f_D) \sim \sin \left[\cos^{-1} \left(\frac{c f_D}{2 V f_0} \right) \right] \quad (74)$$

$$\sim \sqrt{1 - \frac{c^2 f_D^2}{4 V^2 f_0^2}} = \sqrt{1 - f_D^2 / f_{DM}^2}$$

where f_{DM} is the maximum doppler shift.

It should be observed that the calculated chaff return power spectral density is an even function with identical doppler spectra appearing as mirror images at both $+f_0$ and $-f_0$ on the frequency axis. Considering the case of vertical flight, we have plotted the doppler spectrum for an isotropic radar antenna, Rayleigh chaff cloud, and uniform dipole orientation distribution in figure 28. Figure 29 is a similar plot for a $\cos^2 \theta$ antenna pattern, Rayleigh chaff cloud, and uniform dipole orientation distribution.

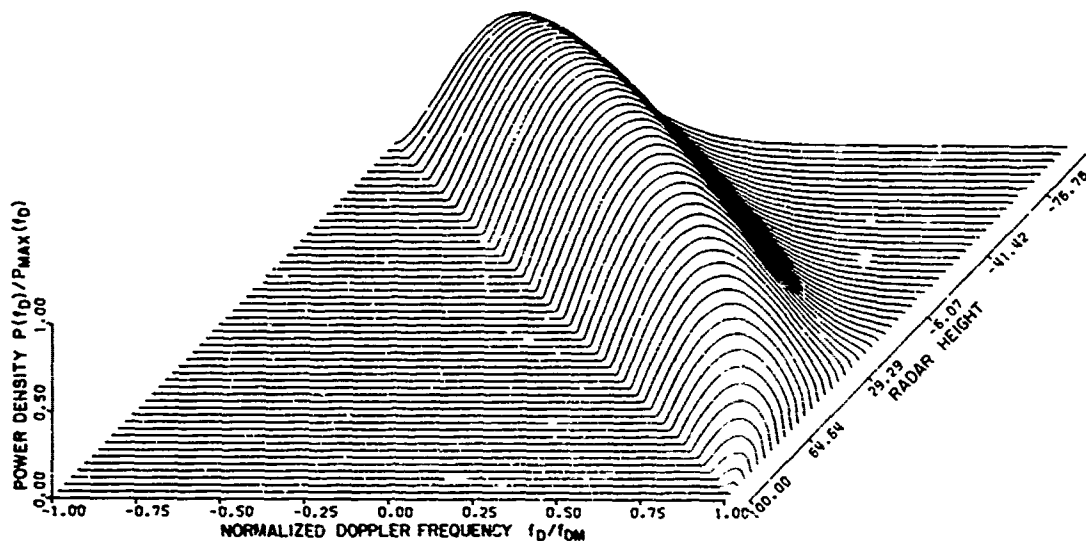


Figure 28. Doppler spectral density function for range-gated response at $d = 100$ m with an isotropic antenna pattern (Rayleigh cloud model, $\alpha = 0.001$) uniformly distributed dipole orientations.

It is relevant to the problem of chaff detection to observe that the return signal to the radar will have the maximum doppler frequency shift and minimum frequency dispersion when the radar first encounters the chaff cloud. At this time, the envelope coefficient of correlation from pulse to pulse will be nearly unity. After the radar range gate is completely submerged in the chaff cloud, the frequency dispersion will reach a maximum and the pulse to

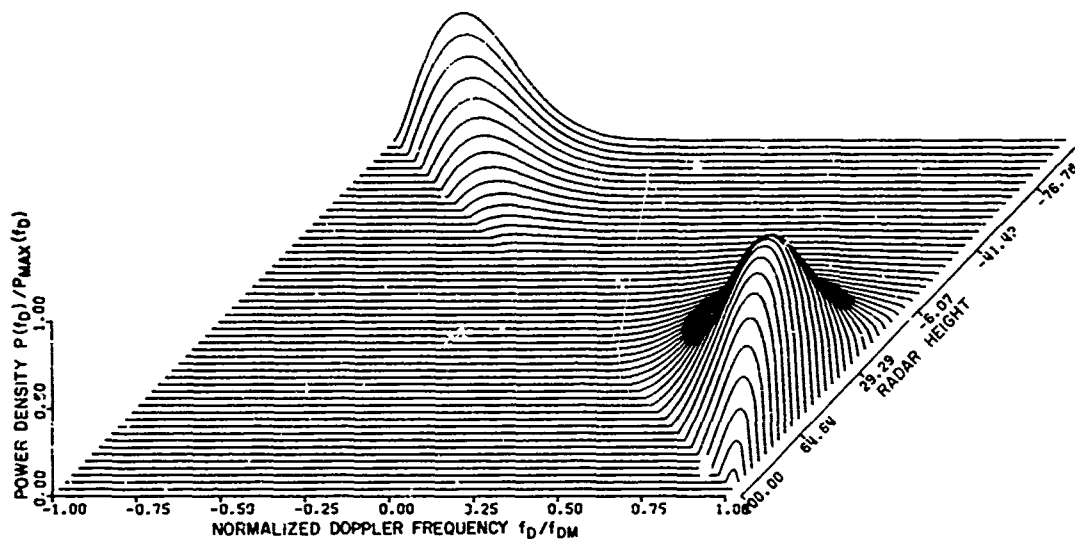


Figure 29. Doppler spectral density function for rc. e-gated response at $d = 100$ m with a $\cos^2\theta$ antenna pattern (Rayleigh cloud model, $a = 0.001$) uniformly distributed dipole orientations

pulse envelope correlation will reach a minimum. For a radar with a high loop sensitivity relative to the chaff return loop attenuation, the initial detection probability will be lower than that obtainable from independent pulse returns. Conversely, for a radar with low loop sensitivity relative to the chaff return loop attenuation, the initial detection probability will be higher than that obtainable from independent pulses.

7. CORRELATION FUNCTION

To calculate second-order probabilities for chaff return powers, we must first obtain the coefficient of correlation at the sampling interval. Since the correlation function for predetection powers is the same, except for a scale factor, as the correlation function for voltages after square-law detection, we obtain both results simultaneously. Recall that the correlation function of the output of a full-wave, square-law device with a gaussian input becomes¹⁰

$$R_y(\tau) \sim \sigma_x^4 + 2R_x^2(\tau). \quad (75)$$

where $R_x(\tau)$ is the input correlation function and $\sigma_x^2 = R_x(0)$. The output coefficient of correlation becomes

$$\rho_y(\tau) = \frac{R_y(\tau) - R_y(\infty)}{R_y(0) - R_y(\infty)} = \frac{R_x^2(\tau)}{\sigma_x^4}. \quad (76)$$

¹⁰Davenport, W. B. and Root, W. L., An Introduction to the Theory of Random Signals and Noise, McGraw-Hill, New York, 1958.

which may be rewritten by using the Weiner-Khinchine relations as

$$\rho_y(\tau) \sim \int_{-\infty}^{\infty} \int_{-\infty}^{\infty} P_x(f') P_x(f-f') e^{2\pi i \tau f} df' df. \quad (77)$$

That is, the coefficient of correlation for the output of a square-law device is the normalized Fourier transform of the self-convolved power spectral density for the backscattered signal. The coefficient of correlation for the output of a square-law device followed by an ideal low-pass filter is the coefficient of correlation for sampled return powers and becomes

$$\rho(\tau) \sim \int_{-f_{DM}}^{f_{DM}} \int_{-\infty}^{\infty} P_x(f') P_x(f-f') e^{2\pi i \tau f} df' df. \quad (78)$$

Thus, from a knowledge of the doppler dispersion spectral density developed in the previous section, the use of equation (78) allows us to readily calculate the return-power coefficient of correlation.

In the case of the uniform density chaff cloud with uniformly distributed dipole orientations, with the range gate completely submerged, and with an isotropic antenna we may apply equation (78) directly to obtain

$$\rho(\tau) = \frac{J_1^2(2\pi f_{DM} \tau)}{(\pi f_{DM} \tau)^2}, \quad (79)$$

where J_1 is the bessel function of the first kind of order one, and $\rho(\tau)$ is the coefficient of correlation for return-power samples separated by the time interval τ .

For the more general cases involving nonuniform cloud densities and/or anisotropic antenna patterns, the direct application of equation (78) will not usually be possible. In such cases, the use of fast Fourier transform (FFT) numerical computing technique as described by Cooley et al.¹³ may be appropriate. The computational procedure involves the self-convolution of the return-signal power spectral density, the separation of the resulting spectrum into low-frequency and high-frequency parts, and application of the FFT to the low-frequency part.

Considering the examples used in the previous section, we have employed the FFT technique and plotted the power correlation functions for the radar height ranging from initial entry of the range cell into the chaff cloud to the total submersion of the range cell in the cloud. The correlation function for a vertical flight path, uniform dipole orientation distribution, Rayleigh chaff cloud, and isotropic antenna is plotted as figure 30. Figure 31 is a similar plot for a $\cos^2\theta$ antenna pattern. Both plots are mean adjusted to zero and the variance at each height normalized as in figures 23 and 24, respectively.

¹³Cooley, J. W., Lewis, P. A., and Welch, P. D., "Application of the Fast Fourier Transform to Computation of Fourier Integrals, Fourier Series, and Convolution Integrals," IEEE Trans, Audio and Electroacoustics, vol. AU-15, No. 2, June 1967.

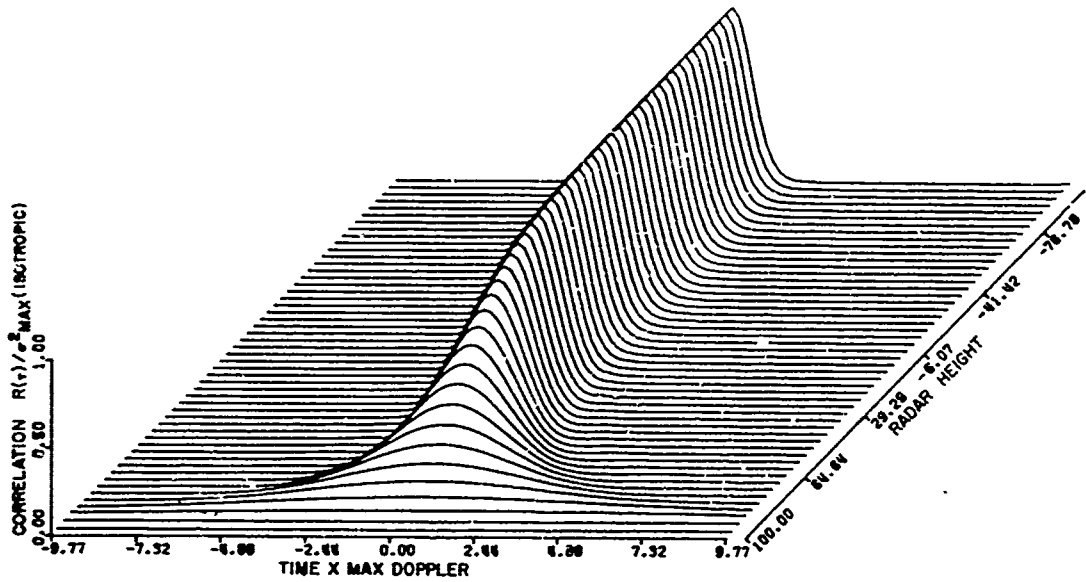


Figure 30. Correlation function for range-gated response at $d = 100$ m with an isotropic antenna pattern (Rayleigh cloud model, $\alpha = 0.001$) uniformly distributed dipole orientations

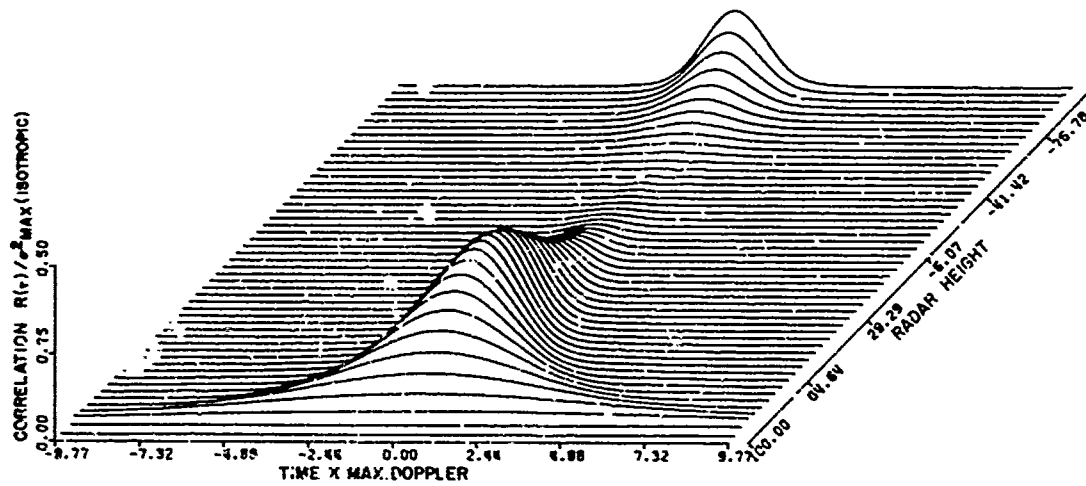


Figure 31. Correlation function for range-gated response at $d = 100$ m with a $\cos^2\theta$ antenna pattern (Rayleigh cloud model, $\alpha = 0.001$) uniformly distributed dipole orientations

From figure 30, we may observe that approximately $5(c/2V)$ rf periods must elapse between essentially uncorrelated samples when the radar is 75 m above the chaff cloud. After the radar has penetrated into the cloud a depth of 100 m, however, approximately four essentially uncorrelated samples may be obtained in the same time interval. Hence, if the detection process involves the incoherent integration of a number of successive pulses and the pulse repetition period is shorter than $5(c/2V)$ rf periods, the fluctuations about the mean of the integrated process will be considerably greater at a height of 75 m than at -100 m.

8. SUMMARY

In this report, we have provided a model for chaff sufficiently general to characterize a diverse set of distribution geometries. Simultaneously, we have retained the requisite simplicity of description so that the methodology of specific calculations is not unnecessarily encumbered. We have introduced and developed the concept of the chaff impulse response, noting that such a function is theoretically fictitious, but recognizing it as a practical approximation for chaff backscatter to a short-pulse radar. A significant difference between the delay time to peak for the chaff impulse response as compared with the rough surface scatter impulse response has been noted.

We have also examined the response to a chaff cloud as viewed from a fixed range cell as the radar moves relative to the cloud. The probability density functions of such a signal have been reviewed, and the spectral density function for this signal in consonance with our chaff cloud model has been derived. Considering square-law detection of this signal, we have obtained the correlation function of the detector output and examined its fluctuation rate as the position of the radar above and within the chaff cloud is varied.

9. LITERATURE CITED

- (1) Chang, S. and Liepa, V., "Measured Back Scattering Cross Section of Thin Wires," The University of Michigan Radiation Laboratory, Report No. 8077-4-T, 1967.
- (2) deBettancourt, J. T., "Bistatic Cross Sections of Cylindrical Wires," Pickard & Burns, Inc., Scientific Report No. 1, P&B Pub. No. 735A, Waltham, Mass., 1961.
- (3) Palermo, C. J. and Bauer, L. H., "Bistatic Scattering Cross Section of Chaff Dipoles with Application to Communications," Proceedings IEEE, Aug. 1965.
- (4) Moore, R. K. and Williams, C. S., "Radar Return at Near-Vertical Incidence," Proceedings IRE, Vol. 45, 1957.
- (5) Siegert, A. and Goldstein, H., "Coherent and Incoherent Scattering from Assemblies of Scatterers," in Propagation of Short Radio Waves, Kerr, D. E., ed., McGraw-Hill, New York, 1951.
- (6) Edison, A. R., Moore, R. K., and Warner, B. D., "Radar Return at Near-Vertical Incidence, Summary Report," Univ. of New Mexico Engineering Experiment Station, Tech. Rep. EE-24, Sept. 1959.

- (7) Rice, S., "Mathematical Analysis of Random Noise," Bell Systems Technical Journal, vol. 23, 1944 and vol. 24, 1945.
- (8) Borison, S. L., "Statistics of the Radar Cross Section of a Volume of Chaff," MIT, Lincoln Laboratory, Group Rep 1965-10, 1965.
- (9) Wong, J. L., Reed, I. S., and Kaprielian, Z. A., "A Model for Radar Echoes from a Random Collection of Rotating Dipole Scatterers," USCEE Report 159, Jan. 1966.
- (10) Davenport, W. B. and Root, W. L., An Introduction to the Theory of Random Signals and Noise, McGraw-Hill, New York, 1958.
- (11) Cooley, J. W., Lewis, P. A., and Welch, P. D., "Application of the Fast Fourier Transform to Computation of Fourier Integrals, Fourier Series and Convolution Integrals," IEEE Trans, Audio and Electroacoustics, vol. AU-15, No. 2, June 1967.

GLOSSARY OF TERMS

- a = radius of the circular cross section of a thin wire chaff dipole.
- C_{η} = proportionality factor for maximum value of the ratio $\bar{\sigma}_{\eta}/\lambda^2$.
- c = speed of light in vacuo.
- d = range gate nominal distance, distance from the radar to chaff dipoles contributing to the return at a specified time.
- Δd = incremental distance, depth of the range resolution cell.
- $E\{\cdot\}$ = statistical expectation operator.
- FFT = fast Fourier transform numerical computing technique.
- f = frequency.
- f_D = doppler frequency shift.
- f_{DM} = maximum doppler frequency shift.
- f_0 = frequency of transmitted wave (center frequency for a narrow band signal).
- G = antenna power gain.
- G_0 = peak value of antenna power gain.
- G_r = receiving antenna power gain.
- G_t = transmitting antenna power gain.
- h = distance from the radar to the chaff cloud top (positive when the radar is above the cloud).

h' = a vertical distance measured from the radar.

l = length of chaff dipole.

$m(\cdot)$ = mean value function of a stochastic process.

n = total number of chaff dipoles contained in the vertical column over each horizontal unit area.

N_v = a Poisson distributed random variable, the number of chaff dipoles contained in region v .

$N(v_p)$ = a Poisson process specifying number of chaff dipoles contained in a region centered on point P .

P_r = backscattered received power, square of envelope of the return signal.

P_r^δ = chaff impulse response function.

P_t = transmitted power, the square of envelope of the transmitted signal.

$P_x(f)$ = power spectral density function of the random process, $X(t)$.

$p(x)$ = first-order probability density function of the random variable, X [stationary random process $X(t)$]

$p_2(X_1, X_2)$ = second-order probability density function of the random variables X_1 and X_2 [random process $X(t_1)$ and $X(t_2)$].

$R(\lambda, \eta)$ = a function of the wavelength λ and the polarization state η

$$R(\lambda, \eta) = \frac{c G_0^2 \lambda^4 C_\eta}{4 (4\pi)^2} .$$

$R_x(\tau)$ = correlation function for the stationary random process $X(t)$.

t = time variable.

v = magnitude of radar velocity.

v_{CH} = mean chaff drift speed.

α = a configuration parameter related to the chaff cloud density gradient.

γ = flight angle between the vertical and the radar velocity vector.

δ = chaff dipole volume density.

δ_m = maximum chaff dipole volume density.

θ = elevation angle of a radar-centered spherical reference frame.

θ' = elevation angle of a dipole-centered spherical reference frame.

λ = nominal wavelength (wavelength associated with the center frequency of a narrow band signal).

$\rho(\tau)$ = coefficient of correlation of a stationary random process.

σ = monostatic radar cross section.

$\bar{\sigma}$ = mean value of the monostatic radar cross section.

$\bar{\sigma}_H$ = mean value of the monostatic radar cross section for a horizontally polarized incident wave.

$\bar{\sigma}_V$ = mean value of the monostatic radar cross section for a vertically polarized incident wave.

σ_η^0 = the chaff volume radar cross section for a η polarized incident wave.

σ_X = standard deviation of random variable X [stationary random process X(t),
 $\sigma_X^2 = R_X(0)$]

τ = time interval between successive samples, the pulse repetition period, the elapsed time since chaff dispersal.

ϕ = azimuth angle of a radar-centered spherical reference frame.

ϕ' = azimuth angle of a dipole-centered spherical reference frame.

Ψ = a uniformly distributed $(0, 2\pi)$ random variable, a random angle of rotation measured in a horizontal plane.

APPENDIX A.—IMPULSE RESPONSE FUNCTIONS

	<u>Page</u>
A-1. Exponential Cloud Model	63
A-1.1 Isotropic Antenna	63
A-1.2 Double-Lobe Antenna	63
A-1.3 Single-Lobe Antenna	64
A-1.4 Hollow-Cone Antenna	64
A-1.5 Horizontal Distribution of Dipole Orientations with Vertically Polarized Wave-Isotropic Antenna	65
A-2. Rayleigh Cloud Model	65
A-2.1 Isotropic Antenna	65
A-2.2 Double-Lobe Antenna	65
A-2.3 Single-Lobe Antenna	66
A-2.4 Hollow-Cone Antenna	66
A-2.5 Horizontal Distribution of Dipole Orientations with Vertically Polarized Wave-Isotropic Antenna	67
A-3. Conclusion	68

Preceding page blank

APPENDIX A. IMPULSE RESPONSE FUNCTIONS

Following are integrated expressions for the impulse response functions developed in section 4 and plotted as figures 10 through 17 (body of report).

A-1. Exponential Cloud Model $\delta = \delta_m (1 - e^{-\alpha(h' - h)})$

Following are mathematical derivations for uniform distribution of dipole orientations or horizontal distribution of dipole orientations with horizontally polarized wave

A-1.1 Isotropic Antenna $G_1 = G_{10}$

$$\begin{aligned}
 P_r^\delta(d) &= \frac{R(\lambda, \eta)}{d^3} \left[d - h + \frac{1}{\alpha} (e^{-\alpha(d+h)} - 1) \right] & -d \leq h \leq d \\
 &= \frac{R(\lambda, \eta)}{d^3} \left[2d + \frac{1}{\alpha} (e^{-\alpha(d-h)} - e^{\alpha(d+h)}) \right], & h < -d \\
 &= 0, & h > d
 \end{aligned}$$

A-1.2 Double-Lobe Antenna $G_2 = G_{20} \cos^2 \theta$

$$\begin{aligned}
 P_r^\delta(d) &= \frac{R(\lambda, \eta)}{d^7} \left\{ \frac{1}{5} (d^5 - h^5) + \left[\frac{24}{\alpha^5} + \frac{24d}{\alpha^4} + \frac{12d^2}{\alpha^3} + \frac{4d^3}{\alpha^2} + \frac{d^4}{\alpha} \right] e^{-\alpha(d-h)} \right. \\
 &\quad \left. - \left[\frac{24}{\alpha^5} + \frac{24h}{\alpha^4} + \frac{12h^2}{\alpha^3} + \frac{4h^3}{\alpha^2} + \frac{h^4}{\alpha} \right] \right\}, & -d \leq h \leq d \\
 &= \frac{R(\lambda, \eta)}{d^7} \left\{ \frac{2}{5} d^5 + \left[\frac{24}{\alpha^5} + \frac{24d}{\alpha^4} + \frac{12d^2}{\alpha^3} + \frac{4d^3}{\alpha^2} + \frac{d^4}{\alpha} \right] e^{-\alpha(d-h)} \right. \\
 &\quad \left. - \left[\frac{24}{\alpha^5} - \frac{24d}{\alpha^4} + \frac{12d^2}{\alpha^3} - \frac{4d^3}{\alpha^2} + \frac{d^4}{\alpha} \right] e^{\alpha(d+h)} \right\}, & h < d \\
 &= 0, & h > d
 \end{aligned}$$

Preceding page blank

A-1.3 Single-Lobe Antenna

$$G_3 = G_{10} \cos^2 \theta, \quad \frac{\pi}{2} \leq \theta \leq \pi$$

$$= 0, \quad 0 \leq \theta < \frac{\pi}{2}$$

$$P_r^\delta(d) = \frac{R(\lambda, \eta)}{d^7} \left\{ \frac{1}{5} (d^5 - h^5) + \left[\frac{24}{\alpha^5} + \frac{24d}{\alpha^4} + \frac{12d^2}{\alpha^3} + \frac{4d^3}{\alpha^2} + \frac{d^4}{\alpha} \right] e^{-\alpha(d-h)} \right.$$

$$\left. - \left[\frac{24}{\alpha^5} + \frac{24h}{\alpha^4} + \frac{12h^2}{\alpha^3} + \frac{4h^3}{\alpha^2} + \frac{h^4}{\alpha} \right], \quad 0 \leq h \leq d \right.$$

$$= \frac{R(\lambda, \eta)}{d^7} \left\{ \frac{1}{5} d^5 + \left[\frac{24}{\alpha^5} + \frac{24d}{\alpha^4} + \frac{12d^2}{\alpha^3} + \frac{4d^3}{\alpha^2} + \frac{d^4}{\alpha} \right] e^{-\alpha(d-h)} \right.$$

$$\left. - \frac{24 e^{\alpha h}}{\alpha^5} \right\}, \quad h < 0$$

$$= 0, \quad h > d$$

A-1.4 Hollow Cone Antenna

$$G_4 = 2 G_{40} \sin \theta \cos \theta, \quad \frac{\pi}{2} \leq \theta \leq \pi$$

$$= 0, \quad 0 \leq \theta < \frac{\pi}{2}$$

$$P_r^\delta(d) = \frac{4 R(\lambda, \eta)}{d^5} \left\{ \frac{1}{3} (d^3 - h^3) + \left[\frac{2}{\alpha^3} + \frac{2d}{\alpha^2} + \frac{d^2}{\alpha} \right] e^{-\alpha(d-h)} \right.$$

$$\left. - \left[\frac{2}{\alpha^3} + \frac{2h}{\alpha^2} + \frac{h^2}{\alpha} \right] \right\} - \frac{4 R(\lambda, \eta)}{d^7} \left\{ \frac{1}{5} (d^5 - h^5) + \left[\frac{24}{\alpha^5} + \frac{24d}{\alpha^4} + \frac{12d^2}{\alpha^3} \right. \right.$$

$$\left. + \frac{4d^3}{\alpha^2} + \frac{d^4}{\alpha} \right] e^{-\alpha(d-h)} - \left[\frac{24}{\alpha^5} + \frac{24h}{\alpha^4} + \frac{12h^2}{\alpha^3} + \frac{4h^3}{\alpha^2} + \frac{h^4}{\alpha} \right] \right\}, \quad 0 \leq h \leq d$$

$$= \frac{4 R(\lambda, \eta)}{d^5} \left\{ \frac{d^3}{3} - \frac{2 e^{\alpha h}}{\alpha^3} + \left[\frac{2}{\alpha^3} + \frac{2d}{\alpha^2} + \frac{d^2}{\alpha} \right] e^{-\alpha(d-h)} \right\}$$

$$- \frac{4 R(\lambda, \eta)}{d^7} \left\{ \frac{d^5}{5} - \frac{24 e^{\alpha h}}{\alpha^5} + \left[\frac{24}{\alpha^5} + \frac{24d}{\alpha^4} + \frac{12d^2}{\alpha^3} + \frac{4d^3}{\alpha^2} \right. \right.$$

$$\left. + \frac{d^4}{\alpha} \right] e^{-\alpha(d-h)} \right\}, \quad h < 0$$

$$= 0, \quad h > d$$

A-1.5 Horizontal Distribution of Dipole Orientations with Vertically Polarized Wave -- Isotropic Antenna

$$G_1 = G_{10}$$

$$\begin{aligned}
 P_r^\delta(d) &= \frac{R(\lambda, \eta)}{d^9} \left\{ \frac{1}{6} (d^6 - h^6) + \left[\frac{120}{\alpha^6} + \frac{120 d}{\alpha^5} + \frac{60 d^2}{\alpha^4} + \frac{20 d^3}{\alpha^3} + \frac{5 d^4}{\alpha^2} + \frac{d^5}{\alpha} \right] e^{-\alpha(d-h)} \right. \\
 &\quad \left. - \left[\frac{120}{\alpha^6} + \frac{120 h}{\alpha^5} + \frac{60 h^2}{\alpha^4} + \frac{20 h^3}{\alpha^3} + \frac{5 h^4}{\alpha^2} + \frac{h^5}{\alpha} \right] \right\}, \quad 0 \leq h \leq d \\
 &= \frac{R(\lambda, \eta)}{d^9} \left\{ \frac{1}{6} (d^6 + h^6) + \left[\frac{120}{\alpha^6} + \frac{120 d}{\alpha^5} + \frac{60 d^2}{\alpha^4} + \frac{20 d^3}{\alpha^3} + \frac{5 d^4}{\alpha^2} + \frac{d^5}{\alpha} \right] e^{-\alpha(d-h)} \right. \\
 &\quad \left. + \left[\frac{120}{\alpha^6} + \frac{120 h}{\alpha^5} + \frac{60 h^2}{\alpha^4} + \frac{20 h^3}{\alpha^3} + \frac{5 h^4}{\alpha^2} + \frac{h^5}{\alpha} \right] - \frac{240 e^{ah}}{\alpha^6} \right\}, \quad -d \leq h < 0 \\
 &= \frac{R(\lambda, \eta)}{d^9} \left\{ \frac{d^6}{3} + \left[\frac{120}{\alpha^6} + \frac{120 d}{\alpha^5} + \frac{60 d^2}{\alpha^4} + \frac{20 d^3}{\alpha^3} + \frac{5 d^4}{\alpha^2} + \frac{d^5}{\alpha} \right] e^{-\alpha(d-h)} \right. \\
 &\quad \left. + \left[\frac{120}{\alpha^6} + \frac{120 d}{\alpha^5} + \frac{60 d^2}{\alpha^4} - \frac{20 d^3}{\alpha^3} + \frac{5 d^4}{\alpha^2} - \frac{d^5}{\alpha} \right] e^{\alpha(d+h)} - \frac{240 e^{ah}}{\alpha^6} \right\}, \quad h < -d \\
 &= 0, \quad h > d
 \end{aligned}$$

A-2 Rayleigh Cloud Model $\delta = na(h' - h)e^{-\alpha/2(h' - h)}$

Following are mathematical derivations for uniform distribution of dipole orientations or horizontal distribution of dipole orientations with horizontally polarized wave

A-2.1 Isotropic Antenna $G_1 = G_{10}$

$$\begin{aligned}
 P_r^\delta(d) &= \frac{R(\lambda, \eta)}{d^5} [1 - e^{-\alpha/2(d-h)^2}], \quad -d \leq h \leq d \\
 &= \frac{R(\lambda, \eta)}{d^3} [e^{-\alpha/2(d+h)^2} + e^{-\alpha/2(d-h)^2}], \quad h < -d \\
 &= 0, \quad h > d
 \end{aligned}$$

A-2.2 Double-Lobe Antenna $G_2 = G_{20} \cos^2 \theta$

$$\begin{aligned}
 P_r^\delta(d) &= \frac{R(\lambda, \eta)}{d^7} \left\{ \left(h^4 + \frac{12 h^2}{\alpha} + \frac{8}{\alpha^2} \right) - \left[d^4 + \frac{4}{\alpha} (d^2 + h d + h^2) \right. \right. \\
 &\quad \left. \left. + \frac{8}{\alpha^2} \right] e^{-\alpha/2(d-h)^2} + \left(4 h^3 + \frac{12 h}{\alpha} \right) \sqrt{\frac{\pi}{2\alpha}} \operatorname{erf} \left[\sqrt{\frac{\alpha}{2}} (d-h) \right] \right\}, \quad -d \leq h \leq d
 \end{aligned}$$

$$\begin{aligned}
&= \frac{R(\lambda, \eta)}{d^7} \left\{ \left[d^4 + \frac{4}{a} (d^2 - h d + h^2) + \frac{8}{a^2} \right] e^{-\alpha/2 (d+h)^2} - \left[d^4 \right. \right. \\
&+ \frac{4}{a} (d^2 + h d + h^2) + \frac{8}{a^2} \left. \right] e^{-\alpha/2 (d-h)^2} + \left(4 h^3 + \frac{12 h}{a} \right) \sqrt{\frac{\pi}{2 a}} \left\{ \operatorname{erf} \left[\sqrt{\frac{\alpha}{2}} (d-h) \right] \right. \\
&+ \left. \left. \operatorname{erf} \left[\sqrt{\frac{\alpha}{2}} (d+h) \right] \right\} \right\}, \quad h < -d \\
&= 0, \quad h > d
\end{aligned}$$

A-2.3 Single-Lobe Antenna

$$\begin{aligned}
G_3 &= G_{30} \cos^2 \theta, \quad \frac{\pi}{2} \leq \theta \leq \pi \\
&= 0, \quad 0 \leq \theta < \frac{\pi}{2}
\end{aligned}$$

$$\begin{aligned}
P_r^s(d) &= \frac{R(\lambda, \eta)}{d^7} \left\{ \left(h^4 + \frac{12 h^2}{a} + \frac{8}{a^2} \right) - \left[d^4 + \frac{4}{a} (d^2 + h d + h^2) \right. \right. \\
&+ \left. \left. \frac{8}{a^2} \right] e^{-\alpha/2 (d-h)^2} + \left(4 h^3 + \frac{12 h}{a} \right) \sqrt{\frac{\pi}{2 a}} \operatorname{erf} \left[\sqrt{\frac{\alpha}{2}} (d-h) \right] \right\}, \quad 0 \leq h \leq d \\
&= \frac{R(\lambda, \eta)}{d^7} \left\{ \left(\frac{4 h^2}{a} + \frac{8}{a^2} \right) e^{-\alpha/2 h^2} - \left[d^4 + \frac{4}{a} (d^2 + h d + h^2) + \frac{8}{a^2} \right] e^{-\alpha/2 (d-h)^2} \right. \\
&+ \left. \left(4 h^3 + \frac{12 h}{a} \right) \sqrt{\frac{\pi}{2 a}} \left\{ \operatorname{erf} \left[\sqrt{\frac{\alpha}{2}} (d-h) \right] + \operatorname{erf} \left[\sqrt{\frac{\alpha}{2}} h \right] \right\} \right\}, \quad h < 0 \\
&= 0, \quad h > d
\end{aligned}$$

A-2.4 Hollow-Cone Antenna

$$\begin{aligned}
G_4 &= 2 G_{40} \sin \theta \cos \theta, \quad \frac{\pi}{2} \leq \theta \leq \pi \\
&= 0, \quad 0 \leq \theta < \frac{\pi}{2}
\end{aligned}$$

$$\begin{aligned}
P_r^s(d) &= \frac{4 R(\lambda, \eta)}{d^5} \left\{ \left(h^2 + \frac{2}{a} \right) - \left(d^2 + \frac{2}{a} \right) e^{-\alpha/2 (d-h)^2} + 2 h \sqrt{\frac{\pi}{2 a}} \operatorname{erf} \left[\sqrt{\frac{\alpha}{2}} (d-h) \right] \right\} \\
&- \frac{4 R(\lambda, \eta)}{d^7} \left\{ \left(h^4 + \frac{12 h^2}{a} + \frac{8}{a^2} \right) - \left[d^4 + \frac{4}{a} (d^2 + h d + h^2) + \frac{8}{a^2} \right] e^{-\alpha/2 (d-h)^2} \right. \\
&+ \left. \left(4 h^3 + \frac{12 h}{a} \right) \sqrt{\frac{\pi}{2 a}} \operatorname{erf} \left[\sqrt{\frac{\alpha}{2}} (d-h) \right] \right\}, \quad 0 \leq h \leq d
\end{aligned}$$

$$\begin{aligned}
P_r^{\delta}(d) &= \frac{R(\lambda, \eta)}{d^5} \left\{ \frac{2}{\alpha} e^{-\alpha/2 h^2} - \left(d^2 + \frac{2}{\alpha} \right) e^{-\alpha/2 (d-h)^2} + 2h \sqrt{\frac{\pi}{2\alpha}} \left(\operatorname{erf} \left[\sqrt{\frac{\alpha}{2}} (d-h) \right] \right. \right. \\
&\quad \left. \left. + \operatorname{erf} \left[\sqrt{\frac{\alpha}{2}} h \right] \right) \right\} - \frac{R(\lambda, \eta)}{d^7} \left\{ \left(\frac{4h^2}{\alpha} + \frac{8}{\alpha^2} \right) e^{-\alpha/2 h^2} - \left[d^4 + \frac{4}{\alpha} (d^2 + h d \right. \right. \\
&\quad \left. \left. + h^2) + \frac{8}{\alpha^2} \right] e^{-\alpha/2 (d-h)^2} + \left(4h^3 + \frac{12h}{\alpha} \right) \sqrt{\frac{\pi}{2\alpha}} \left(\operatorname{erf} \left[\sqrt{\frac{\alpha}{2}} (d-h) \right] \right. \right. \\
&\quad \left. \left. + \operatorname{erf} \left[\sqrt{\frac{\alpha}{2}} h \right] \right) \right\}, \quad h < 0 \\
&= 0, \quad h > d
\end{aligned}$$

A-2.5 Horizontal Distribution of Dipole Orientations with Vertically Polarized Wave - Isotropic Antenna

$$G_1 = C_{10}$$

$$\begin{aligned}
P_r^{\delta}(d) &= \frac{R(\lambda, \eta)}{d^9} \left\{ \left(h^5 + \frac{20h^3}{\alpha} + \frac{40h}{\alpha^2} \right) - \left[d^5 + \frac{5}{\alpha} (d^3 + h d^2 + h^2 d + h^3) \right. \right. \\
&\quad \left. \left. + \frac{5}{\alpha^2} (3d + 5h) \right] e^{-\alpha/2 (d-h)^2} + \left(5h^4 + \frac{30h^2}{\alpha} + \frac{15}{\alpha^2} \right) \sqrt{\frac{\pi}{2\alpha}} \operatorname{erf} \left[\sqrt{\frac{\alpha}{2}} (d-h) \right] \right\}, \quad 0 \leq h \leq d \\
&= \frac{R(\lambda, \eta)}{d^9} \left\{ 10 \left(\frac{h^3}{\alpha} + \frac{5h}{\alpha^2} \right) e^{-\alpha/2 h^2} - \left(h^5 + \frac{20h^3}{\alpha} + \frac{40h}{\alpha^2} \right) - \left[d^5 \right. \right. \\
&\quad \left. \left. + \frac{5}{\alpha} (d^3 + h d^2 + h^2 d + h^3) + \frac{5}{\alpha^2} (3d + 5h) \right] e^{-\alpha/2 (d-h)^2} + 5 \left(h^4 + \frac{6h^2}{\alpha} \right. \right. \\
&\quad \left. \left. + \frac{3}{\alpha^2} \right) \sqrt{\frac{\pi}{2\alpha}} \left(\operatorname{erf} \left[\sqrt{\frac{\alpha}{2}} (d-h) \right] + 2 \operatorname{erf} \left[\sqrt{\frac{\alpha}{2}} h \right] \right) \right\}, \quad -d \leq h < 0 \\
&= \frac{R(\lambda, \eta)}{d^9} \left\{ 10 \left(\frac{h^3}{\alpha} + \frac{5h}{\alpha^2} \right) e^{-\alpha/2 h^2} + \left[d^5 - \frac{5}{\alpha} (h^3 - h^2 d + h d^2 - d^3) \right. \right. \\
&\quad \left. \left. - \frac{5}{\alpha^2} (5h - 3d) \right] e^{-\alpha/2 (d+h)^2} - \left[d^5 + \frac{5}{\alpha} (d^3 + h d^2 + h^2 d + h^3) \right. \right. \\
&\quad \left. \left. + \frac{5}{\alpha^2} (3d + 5h) \right] e^{-\alpha/2 (d-h)^2} + 5 \left(h^4 + \frac{6h^2}{\alpha} + \frac{3}{\alpha^2} \right) \sqrt{\frac{\pi}{2\alpha}} \right. \\
&\quad \left. \left(\operatorname{erf} \left[\sqrt{\frac{\alpha}{2}} (d-h) \right] - \operatorname{erf} \left[\sqrt{\frac{\alpha}{2}} (d+h) \right] + 2 \operatorname{erf} \left[\sqrt{\frac{\alpha}{2}} h \right] \right) \right\}, \quad h < -d \\
&= 0, \quad h > d
\end{aligned}$$

A-3. Conclusion

Although the exponential chaff cloud model leads to an inverse square range attenuation law in the limit $h \rightarrow \infty$, the Rayleigh chaff cloud model is bounded above by an inverse cube range attenuation law. In this respect, the Rayleigh model more closely resembles surface distributed scatterers.